ACS NANO

Cite This: ACS Nano 2019, 13, 3992–4007

www.acsnano.org

ARTICLE

Intrinsic Antibacterial Activity of Nanoparticles Made of β-Cyclodextrins Potentiates Their Effect as Drug Nanocarriers against Tuberculosis

Arnaud Machelart,[†] Giuseppina Salzano,[‡] Xue Li,[‡] Aurore Demars,[§] Anne-Sophie Debrie,[†] Mario Menendez-Miranda,[‡] Elisabetta Pancani,[‡] Samuel Jouny,[†] Eik Hoffmann,[†] Nathalie Deboosere,[†] Imène Belhaouane,[†] Carine Rouanet,[†] Sophie Simar,[∥] Smaïl Talahari,[∥] Valerie Giannini,[⊥] Baptiste Villemagne,[#] Marion Flipo,[#] Roland Brosch,[⊥] Fabrice Nesslany,[∥] Benoit Deprez,[#] Eric Muraille,[§,¶] Camille Locht,[†] Alain R. Baulard,[†] Nicolas Willand,[#] Laleh Majlessi,[⊥,□] Ruxandra Gref,*[,‡] and Priscille Brodin*[,†]

[†]Université de Lille, CNRS, INSERM, CHU Lille, Institut Pasteur de Lille, U1019 - UMR 8204 - CIIL - Center for Infection and Immunity of Lille, F-59000 Lille, France

[‡]Université Paris Sud, Université Paris-Saclay, CNRS, UMR 8214 - Institute for Molecular Sciences of Orsay (ISMO), F-91405 Orsay, France

[§]Research Unit in Microorganisms Biology (URBM), Laboratory of Immunology and Microbiology, Université de Namur, Narilis, B-5000 Namur, Belgium

[∥]Université de Lille, Institut Pasteur de Lille, EA 4483, F-59000 Lille, France

[⊥]Institut Pasteur, Unit for Integrated Mycobacterial Pathogenomics, Paris, CNRS UMR 3525, 25 Rue du Dr. Roux, F-75015 Paris, France

[#]Université de Lille, INSERM, Institut Pasteur de Lille, U1177 - Drugs and Molecules for living Systems, F-59000 Lille, France

[¶]Laboratory of Parasitology, Faculty of Medicine, Université Libre de Bruxelles, B-1070 Brussels, Belgium

Supporting Information

ABSTRACT: **Multi-drug-resistant tuberculosis (TB) is a major public health problem, concerning about half a million cases each year. Patients hardly adhere to the current strict treatment consisting of more than 10 000 tablets over a 2-year period. There is a clear need for efficient and better formulated medications. We have previously shown that nanoparticles made of cross-linked poly-β-cyclodextrins (pβCD) are efficient vehicles for pulmonary delivery of powerful combinations of anti-TB drugs. Here, we report that in addition to being efficient drug carriers, pβCD nanoparticles are endowed with intrinsic antibacterial properties. Empty pβCD nanoparticles are able to impair *Mycobacterium tuberculosis* (Mtb) establishment after pulmonary administration in mice. pβCD hamper colonization of macrophages by Mtb by interfering with lipid rafts, without inducing toxicity. Moreover, pβCD provoke macrophage apoptosis, leading to depletion of infected cells, thus creating a lung microenvironment detrimental to Mtb persistence. Taken together, our results suggest that pβCD nanoparticles loaded or not with antibiotics have an antibacterial action on their own and could be used as a carrier in drug regimen formulations effective against TB.**

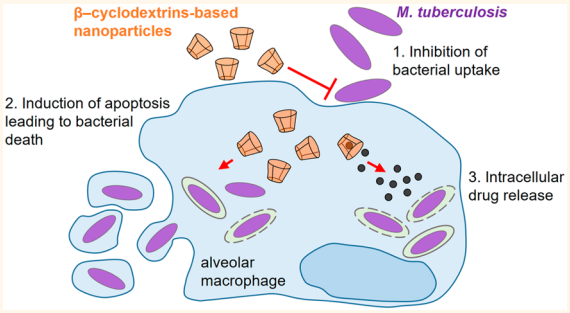

KEYWORDS: *tuberculosis, cyclodextrins, drug nanocarrier, antibacterial activity, host-directed therapy*

Pulmonary tuberculosis (TB), caused by *Mycobacterium tuberculosis* (Mtb), kills 1.3 million HIV-negative and an additional 374 000 HIV-positive people in the world,

Received: October 16, 2018
Accepted: March 1, 2019
Published: March 1, 2019

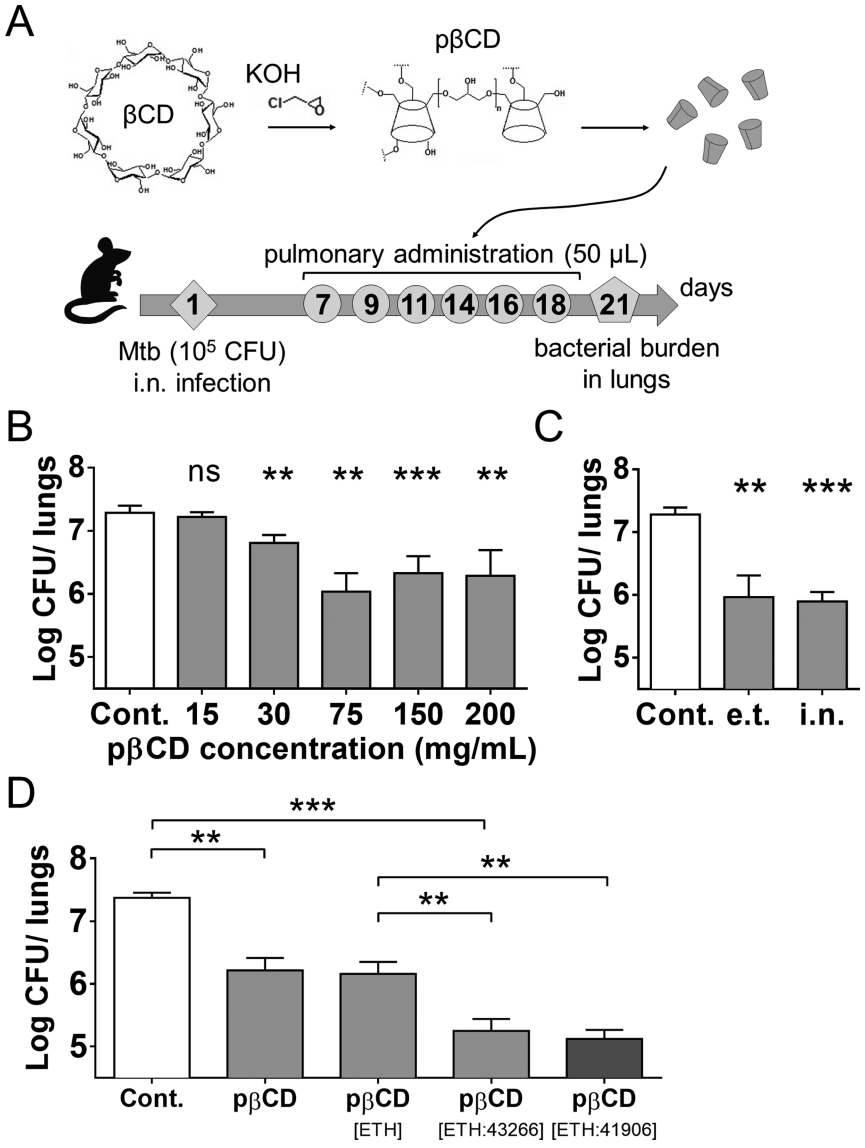

Figure 1. Assessment of the effect of pβCD on the lung mycobacterial load in Mtb-challenged mice. (A) Experimental design: BALB/c mice were anesthetized and i.n. inoculated with 10^5 CFU of Mtb H37Rv strain contained in 20 μL of PBS. At days 7, 9, 11, 14, 16, and 18 postchallenge, mice received administrations of 50 μL of pβCD of various concentrations *via* the e.t. route by use of a microsprayer device that generated aerosolization directly into the lungs. At day 21 postchallenge, lungs were harvested for determination of bacterial burden by CFU counting. (B) Mice received 6 inoculations of 50 μL of pβCD preparations at defined concentrations by the e.t. route before pulmonary bacterial load was evaluated at day 21 postchallenge. (C) Comparison of the impact of pβCD (6 × 50 μL at 150 mg/mL) on Mtb pulmonary load administrated by the i.n. route or by the e.t. route after i.n. infection. (D) Comparison of the effect of the administration of unloaded pβCD and pβCD loaded with ETH alone, [ETH:BDM43266] or [ETH:BDM41906] (6 × 50 μL at 150 mg/mL of pβCD). Data are presented as mean ± SEM and are representative of at least two independent experiments. Symbols ** and * denote $p < 0.01$ and $p < 0.001$, respectively.**

annually.[1] Although TB mortality has decreased over the past 15 years due to implementation of improved TB control programs and strategies, the continuous emergence of multi-drug-resistant (MDR) and extensively drug-resistant (XDR) TB remains highly alarming. New means to fight MDR- and XDR-TB are urgently needed. The current regimen for the treatment of drug-sensitive TB relies on a six-month course of four drugs to be taken orally on a daily basis: isoniazid (INH), rifampicin (RIF), ethambutol (EMB), and pyrazinamide (PZA). Lack of patient compliance and individual host variability in drug pharmacokinetics have led to the development of MDR-TB cases. Treatment of MDR-TB requires two years of second-line antibiotics, such as ethionamide (ETH), fluoroquinolones, and aminoglycosides, which are less effective and cause more severe side effects, whereby the cure rates remain desperately low.[2]

Mtb is a professional pathogen that initially invades and replicates essentially inside phagocytes, such as alveolar and interstitial macrophages. Intracellular Mtb subverts the microbicidal properties of macrophages, which may lead to inefficient containment and development of TB pathology.[3]

Lungs are the major infection site of Mtb transmitted by human-to-human aerogenic spread. In this organ, ingestion and replication of Mtb leads to immune cell recruitment and formation of granulomas, which is a hallmark of the antimycobacterial immune response. The granuloma is composed of an organized aggregation of cells including infected and noninfected macrophages, dendritic cells, inflam-

DOI: 10.1021/acsnano.8b07902
ACS Nano 2019, 13, 3992−4007

matory monocytes and neutrophils, and natural killers and lymphocytes. To exert their activity, antimycobacterial drugs must reach granulomas and express their sterilizing activity within the phagosomes of the innate immune cells in which the bacilli reside.[4] If the bacterial growth is not sufficiently controlled, necrotic tissue lesions can become caseous to form cavities, from which Mtb may be disseminated to other parts of the lung parenchyma. This leads to the initiation of secondary infectious sites, Mtb release to the airways, and thereby transmission to new hosts.

Local administration of anti-TB drugs directly into the lung is an attractive strategy to improve the efficacy of current TB treatment and to reduce systemic side effects. It should also be beneficial in preventing bacterial dissemination and disease establishment by targeting more efficiently infected macrophages, thus reducing administered doses.[5] Nanotechnologies as therapeutic tools to fight microbial resistance, especially against tuberculosis, have been proposed as an effective approach.[6−10] For example, the use of nanoparticles (NPs) allows the administration of poorly soluble drugs into the lungs.[11−13] We recently described that coencapsulation of ETH together with the booster of its bioactivation, called Booster BDM41906,[14] in nanoparticles made of cross-linked poly-β-cyclodextrins (pβCD) overcame the drawbacks related to the strong tendency of ETH to crystallize and to the low solubility of the Booster in aqueous media.[13] Interestingly, pβCD allowed an efficient one-step incorporation of both ETH and Booster by a "green" procedure, which means that no organic solvents were used in the process. Importantly, as we previously described, treatment of Mtb-exposed mice with pβCD loaded with ETH and BDM41906 was shown to lead to a significant decrease of the mycobacterial burden in lungs, similar to that generated by the first-line reference drug INH.[13]

Here, we also investigated the antimycobacterial activity of unloaded pβCD NPs and showed that their pulmonary administration in mice exposed to Mtb results in decreased lung mycobacterial burden compared to nontreated control mice. These results seem to be linked to the finding that pβCD disrupt cell surface lipid rafts and thereby counteract bacterial host cell invasion. Moreover, pβCD induce apoptotic cell death in murine macrophages as well as *in vivo*, which may contribute to the depletion of alveolar macrophages, a main Mtb reservoir. The effect of unloaded NPs against Mtb replication *in vivo* appeared to be rather specific for pβCD. Furthermore, unloaded pβCD were able to impact Mtb but not other bacterial pulmonary pathogens. Taken together, our findings argue for the use of pβCD in drug regimen formulations as an effective tool against TB.

RESULTS AND DISCUSSION

Intrinsic Properties of pβCD against Mtb Growth *in Vivo*. To study the possible impact of unloaded pβCD on the control of Mtb growth *in vivo*, we used a mouse model of acute Mtb infection. BALB/c mice (n = 4/group) were inoculated with 10^5 CFU/mouse of Mtb H37Rv *via* the intranasal (i.n.) route (Figure 1A). The i.n. route of infection was chosen because it is currently widely used[15] and was approved by our animal ethics committee. Mice were then left for 7 days to allow a 1-log increase of Mtb load in the lungs. From day 7 on, and every second day, groups of mice received *via* the endotracheal route (e.t.), by use of a microsprayer device,[13] 50 μL/mouse of diverse concentrations of pβCD, ranging from 15 to 200 mg/mL. These doses are equivalent to 30 to 400 mg/kg of body weight. Compared to untreated mice, on day 21 postchallenge, the animals that had received pβCD displayed decreased pulmonary mycobacterial load by 1-log for all concentrations $\geq$ 30 mg/mL ($p < 0.01$) (Figure 1B). Therefore, it seems that pβCD alone had an intrinsic antimycobacterial effect *in vivo*.

We next examined whether the route of administration had an impact on this activity. The antimycobacterial effect of the same pβCD dose (50 μL of 150 mg/mL) was compared between the e.t. and i.n. routes, using the same regimen as detailed in Figure 1A. A similar decrease in mycobacterial load was detected for both delivery routes by comparison with untreated controls, showing that the two routes of administration can both be equivalently used for further studies (Figure 1C).

We then determined whether the intrinsic antimycobacterial activity of pβCD could synergize with that of the combination of anti-TB drugs when given directly into the lungs. To this end, we investigated the administration of pβCD loaded with both ETH and Booster. Briefly, ETH is a pro-drug that requires bioactivation, mediated by the bacterial mono-oxygenase EthA. This enzyme is under the control of the repressor EthR.[16] Booster molecules induce conformational changes in EthR, resulting in the inhibition of its repressor activity and thereby an enhancement of ETH activity.[14] As previously described, BDM43266, which has been optimized through fragment screening and structure-based design, allows an increase by 10-fold of the activity of ETH against Mtb growth *in vitro*.[17] BDM43266 was thus co-loaded with ETH into pβCD using the previously described conditions of encapsulation.[18] Briefly, powders of the two lipophilic drugs were mixed with suspensions of pβCD at 150 mg/mL overnight, resulting in their spontaneous incorporation in the hydrophobic cavities of the pβCD. This method has the advantage of avoiding the use of organic solvents. Moreover, the drugs were incorporated at the molecular state and did not crystallize upon storage, which is usually an issue with ETH alone. In a previous study with two hydrophobic molecules, drug release from CD-based materials was found to be related in an equilibrium established between free and incorporated drug *in vitro*. We expect the same mechanism to occur for ETH and Booster in alveolar macrophages, which will be investigated in depth in a future study.[19]

Six administrations of pβCD loaded with ETH alone *via* the e.t. route induced a decrease of the bacterial load similarly to that upon administration of pβCD alone, showing that, as expected, delivery of ETH at this low concentration had no antibacterial properties (Figure 1D). Moreover, the administration of pβCD co-loaded with both drugs ETH and BDM43266 ([ETH:43266]) in Mtb-challenged mice led to a significant decrease ($p < 0.05$) of the pulmonary bacterial load by 1 log, compared to the group that received ETH only. These results first showed that BDM43266 had an effective boosting effect on ETH. Second, pβCD were able to deliver sufficient amounts of ETH and BDM43266 *in vivo*. We next compared the boosting efficacy of BDM43266 with that of BDM41906, which we previously reported. No difference was observed concerning the boosting efficacy between BDM41906 and BDM43266. We observed that both Boosters exerted similar effects in our model of infection, suggesting that they should be considered as potent drug candidates for future anti-TB investigations.

The antibacterial activity of NPs is an intense area of research,[20−22] but to the best of our knowledge, only metal nanoparticles, such as silver-, gold-, iron-, or copper-based ones, were shown to promote pathogen eradication.[23−25] However,

DOI: 10.1021/acsnano.8b07902
ACS Nano 2019, 13, 3992−4007

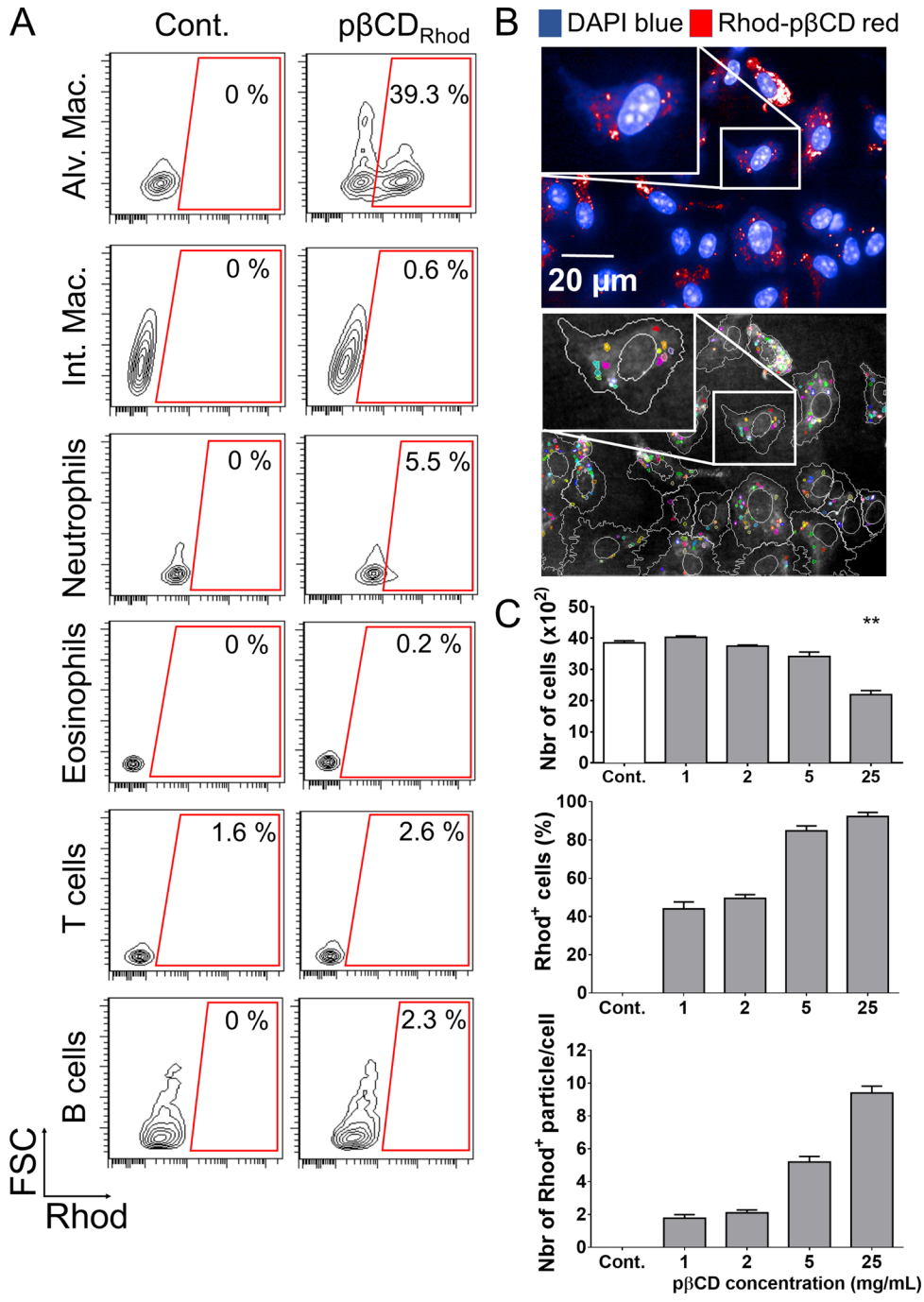

Figure 2. pβCD invade preferentially alveolar macrophages. (A) BALB/c mice received one e.t. administration of rhodamine-coupled pβCD (50 μL of 150 mg/mL) and were euthanized 2 h postadministration to identify cells that internalized nanoparticles by flow cytometry. The following cell types were discriminated: alveolar macrophages (CD11c$^+$ F4/80$^+$ SiglecF$^+$), interstitial macrophages (F4/80$^+$ CD11c^{int} SiglecF$^-$), neutrophils (CD11b$^+$ Ly6G$^+$), eosinophils (SiglecF$^+$ CD11c$^-$), T cells (CD3$^+$), and B cells (B220$^+$ MHCII$^+$). Data represent FSC *vs* Rhod plots of selected populations of one representative mouse in two independent experiments. (B, top image) BMDM originated from BALB/c were incubated 24 h with rhodamine-coupled pβCD before fixation and staining with DAPI in order to label the nuclei for confocal microscopy (scale bar: 20 μm). (B, bottom image) Using Columbus software, images were segmented to delimit cells (white) and Rhod$^+$ pβCD (color). (C) Fields were analyzed to quantify the total number of cells, the percentage of cells interacting with pβCD, and the number of nanoparticles per cell. Data are presented as mean ± SEM and are representative of two independent experiments. ** denotes $p < 0.01$.

concerns can be raised upon repetitive administration of metal-based NPs in pathologies such as TB.

Altogether, this interesting and unexpected result shows that pβCD, when administered directly into the lungs, exert two beneficial actions: (i) making it possible to administer poorly soluble anti-TB drugs without using organic solvents and to transport them to the lungs, the main site of infection, and (ii) potentiating the antimycobacterial effect of these drugs with which they synergize through their intrinsic antimycobacterial property.

Indeed, drug administration into the lungs bypasses limitations of some current TB drugs, which are given orally.

DOI: 10.1021/acsnano.8b07902
ACS Nano 2019, 13, 3992−4007

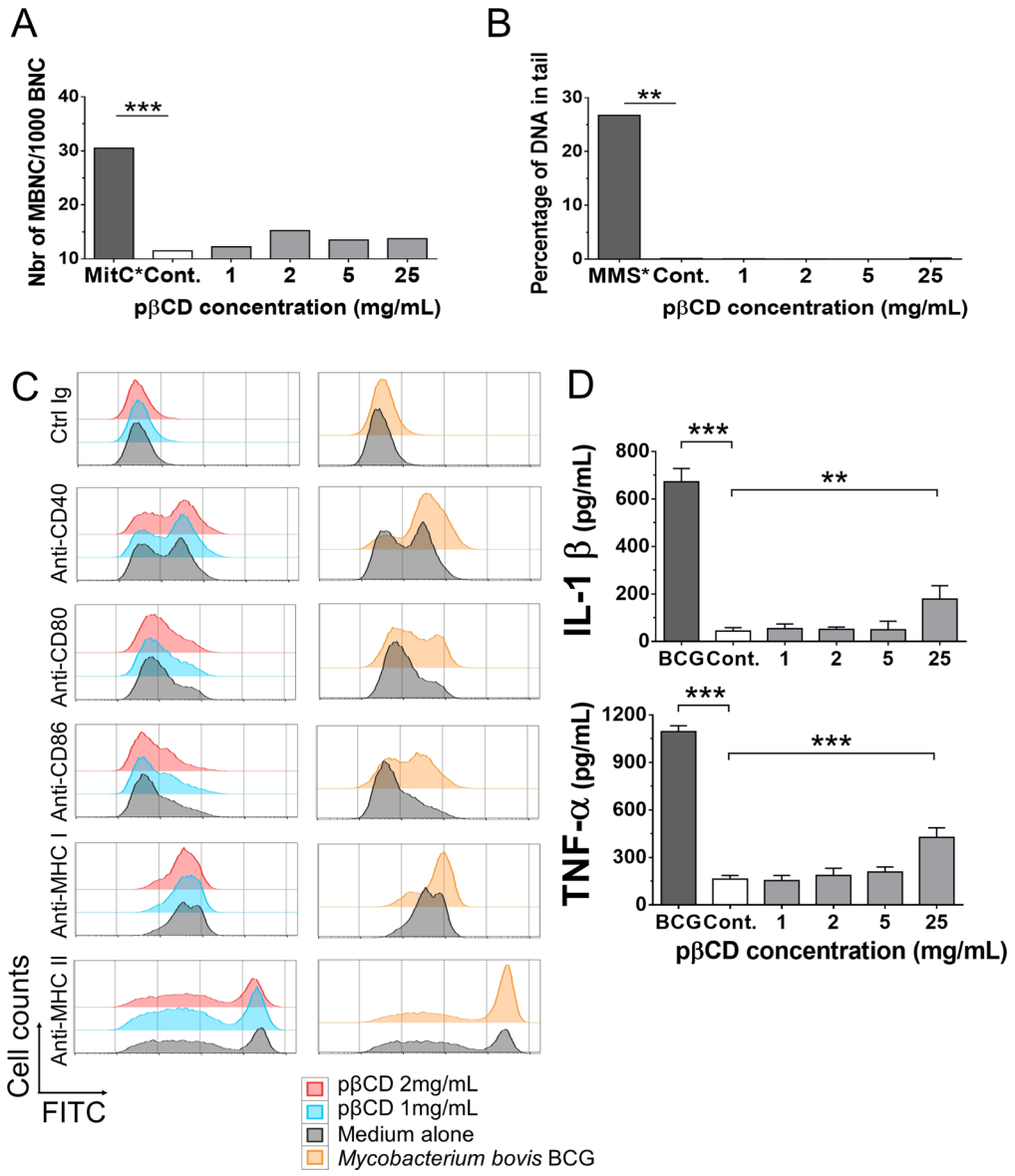

Figure 3. pβCD are not genotoxic and poorly induce pro-inflammatory responses. (A, B) THP1 cells were incubated for 24 h with different concentrations of pβCD for the evaluation of genotoxicity. The micronucleus assay (A) was used to detect any damage that occurred during cell division (mitomycin was used as positive control), while the comet assay (B) was used to evaluate DNA strand breaks (methyl methanesulfonate was used as positive control). (C) BMDC were incubated overnight with pβCD or were inoculated with BCG (MOI = 1), as a positive control. After overnight incubation, cells were stained with FITC-conjugated antibodies. The FITC signal gated on CD11c$^+$ cells shows the surface expression level of co-stimulatory molecules (CD40, CD80, CD86) and MHC-I or MHC-II molecules, as phenotypic dendritic cell maturation markers. (D) As a hallmark of functional dendritic cell maturation, IL-1β and TNF-α were quantified by ELISA in the supernatants of the same cultures, described in (C). Symbols ** and * denote $p < 0.01$ and $p < 0.001$, respectively.**

Besides, when a patient with active TB sneezes, coughs, or spits, droplets containing Mtb can be inhaled by surrounding individuals, who can become infected. The main advantages of the drug administration directly into the lungs are that (i) bacteria could be rapidly eradicated and (ii) Mtb spreading to other cells could be prevented, which is considered as a main strategy to eradicate infection.[4,26−28]

pβCD Are Engulfed by Alveolar Macrophages after Administration. The discovery of the intrinsic antibacterial ability of pβCD prompted us to explore the type of lung cells that could be impacted by this effect. Rhodamine B-conjugated pβCD (Rhod-pβCD) were therefore administered to mice *via* the e.t. route. Diverse cell subsets, including alveolar or interstitial macrophages, neutrophils, eosinophils, T cells, and B lymphocytes, were then examined by flow cytometry for the presence of fluorescent pβCD. Two hours after administration, Rhod-pβCD were preferentially located in alveolar macrophages (CD11c$^+$ F4/80$^+$ SiglecF$^+$) with approximatively 40% of these cells emitting the rhodamine B fluorescent signal (hence referred as Rhod$^+$) (Figure 2A). Taken together, these observations showed that, at early time points following inoculation, pβCD were mainly internalized by alveolar macrophages in mouse lungs, which are among the main cells used by Mtb as a reservoir. This property is of main importance for the delivery of anti-TB drugs. Indeed, the ability for chemical entities to reach Mtb-containing lesions has recently been demonstrated to be an important parameter to take into account during their development.[4] Moreover, having a class of NPs that

DOI: 10.1021/acsnano.8b07902
ACS Nano 2019, 13, 3992−4007

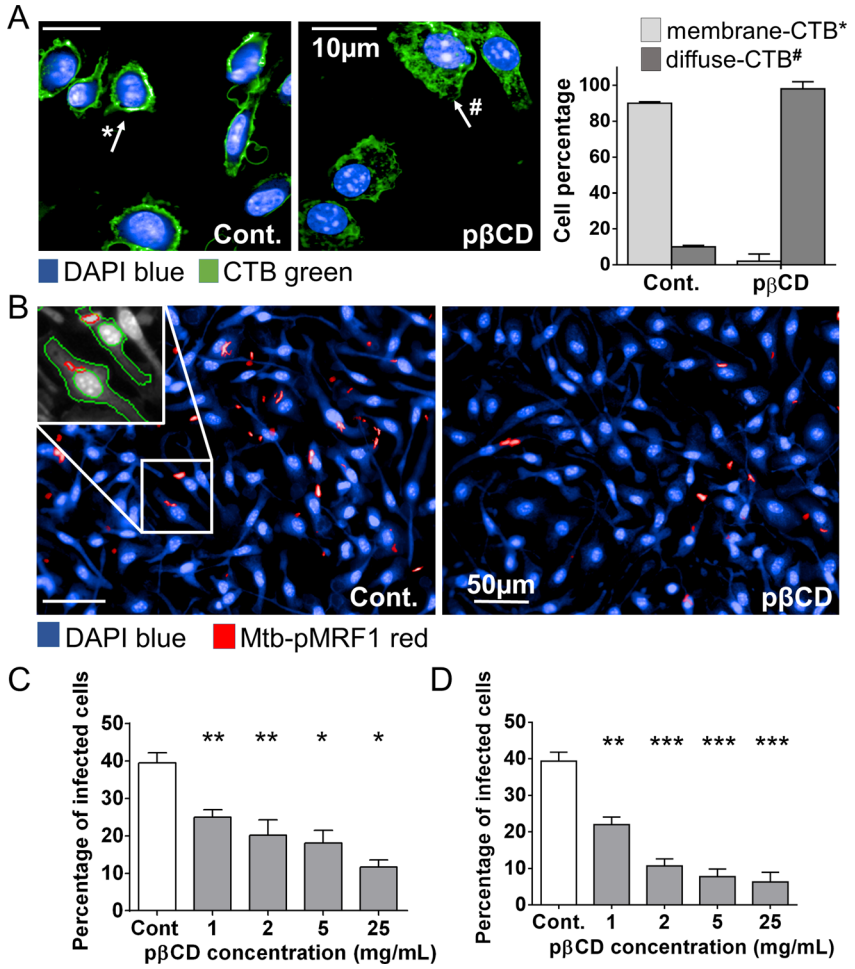

Figure 4. pβCD disturb lipid raft integrity of macrophages and prevent Mtb uptake. BMDM were incubated overnight with pβCD at different concentrations and then fixed with formalin. (A) Effect of pβCD on cholesterol distribution at the plasma membrane in BMDM. Typical images obtained by automated confocal microscopy (pβCD: 16 h at 2 mg/mL) and related quantification. CTB-FITC- and DAPI-labeled nuclei shown in green and blue, respectively. Scale bar: 10 μm. (B, C, D) BMDM were incubated with different concentrations of pβCD for 2 or 16 h prior to infection with red-fluorescent Mtb. (B) Typical images of H37Rv-pMRF1- and DAPI-labeled nuclei are shown in red and blue, respectively (pβCD: 16 h at 5 mg/mL). Scale bar: 50 μm. Percentage of Mtb-infected BMDM (2 h (C) or 16 h (D) postinfection) upon pre-incubation with pβCD. Data are presented as mean ± SEM and are representative of two independent experiments. Symbols *, **, and * denote $p < 0.05$, $p < 0.01$, and $p < 0.001$, respectively.**

acts on the interactions between bacteria and the host allows opportunities for the development of macrophage-targeted host-directed therapies.

The efficient uptake of pβCD by macrophages was further supported by using murine bone-marrow-derived macrophages (BMDM), as typical surrogate cells used in *in vitro* infection experiments. BMDM were incubated with various concentrations of Rhod-pβCD for 24 h, washed, and imaged by confocal microscopy (Figure 2B, top image). Using the image-analysis software Columbus, all images were segmented to delimit each cell and each intracellular $Rhod^+$ nanoparticle (Figure 2B, bottom image). These analyses revealed that more than 80% of the cells had phagocytosed pβCD when added at concentrations of 5 and 25 mg/mL (Figure 2C). Of note, at lower concentrations of pβCD tested (2 mg/mL), 50% of the cells contained approximately two $Rhod^+$ NPs, highlighting the strong capacity of macrophages to internalize pβCD. The number of BMDM per well was also determined (Figure 2C), and this parameter informs on the cytotoxicity of pβCD. There was no difference in cell number for concentrations up to 5 mg/mL compared to control nontreated cells, clearly showing that pβCD are not cytotoxic. However, we observed a 40% decrease of the number of cells for samples incubated with pβCD at 25 mg/mL, suggesting that at this very high concentration pβCD induced cell death. It is important to mention that this concentration is likely never reached in lungs of mice. Indeed, with an administration of 50 μL of a solution containing 150 mg/mL of pβCD, mice received approximately 7.5 mg within lungs, covering a pulmonary volume of approximately 1 mL. The possible genotoxic properties of pβCD are further investigated in the following section.

pβCD Are Not Genotoxic and Have Poor Pro-inflammatory Properties. It is generally admitted that βCD are not genotoxic.[23−25,29] To determine whether the pβCD used in this study share the same properties, their possible genotoxic properties were evaluated on differentiated human macrophage-like THP1 cells, incubated for 24 h with pβCD and processed for the formation of micronuclei, an indicator of chromosomal damage, or for the "*comet*" assay, which measures DNA strand breaks.[30,31] Results showed that pβCD induced neither micronuclei (Figure 3A) nor DNA damage (Figure 3B) in

DOI: 10.1021/acsnano.8b07902
ACS Nano 2019, 13, 3992−4007

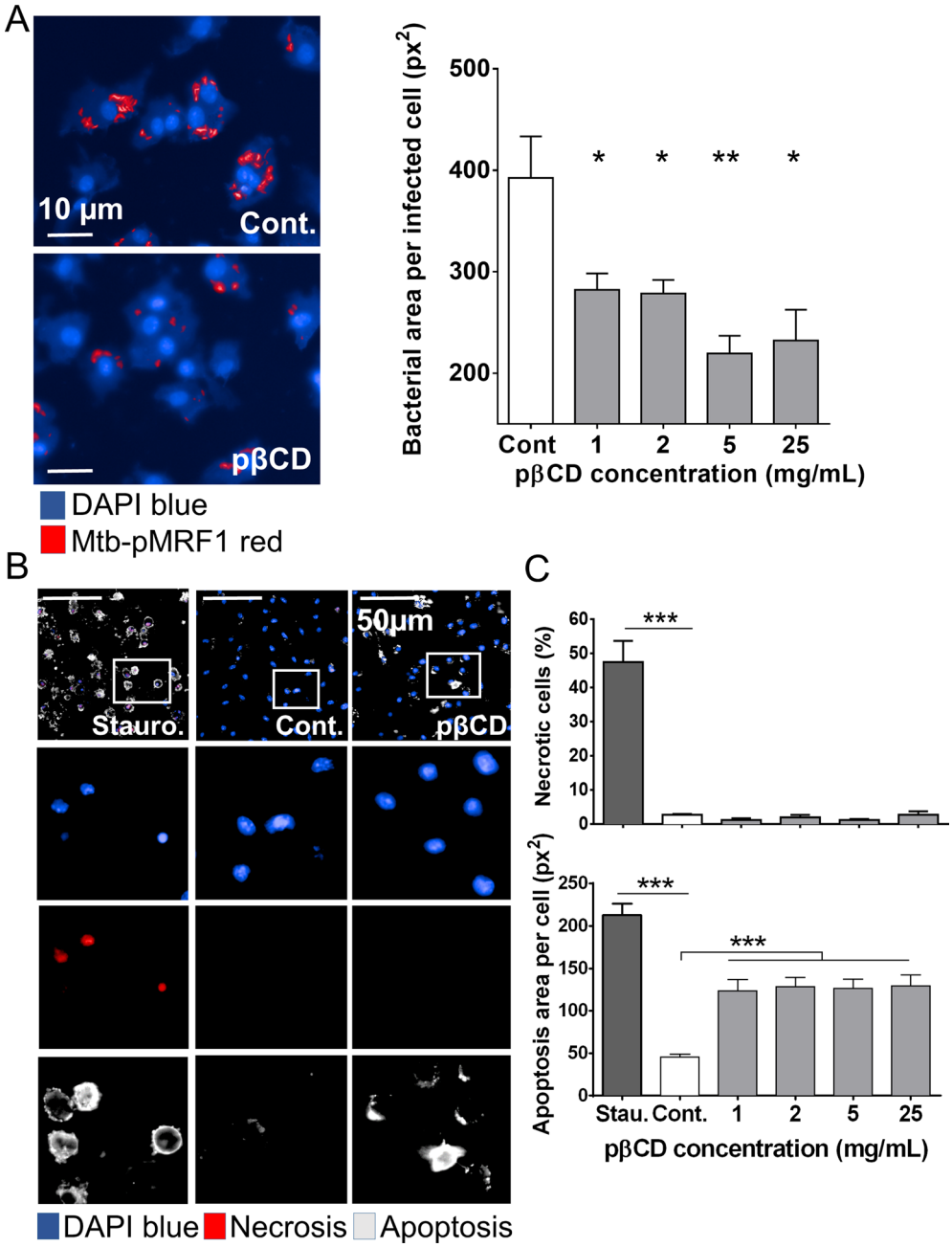

Figure 5. pβCD impair bacterial replication and induce macrophage apoptosis. (A) BMDM were infected with red fluorescent Mtb (Mtb-pMRF1) for 4 h before being incubated for 5 days with pβCD. (Left panel) Typical images of Mtb-infected BMDM upon a 5-day incubation of pβCD at 2 mg/mL. H37Rv-pMRF1- and DAPI-labeled nuclei are shown in red and blue, respectively. Scale bar: 10 µm. (Right panel) Image-based quantification of Mtb replication represented by the bacterial area per infected cells. Cont. corresponds to samples incubated with water. (B, C) Effect of pβCD on necrosis/apoptosis induction in BMDM. (B) Typical images (pβCD: 16 h at 2 mg/mL) and (C) related quantification. DAPI-labeled nuclei are shown in blue. This method allows the detection of early apoptotic cells (positive for annexin V, gray), necrotic cells (positive for DNA intercalating dye, red), and late apoptotic cells (positive for both markers). Staurosporine was used as positive control. Scale bar: 50 µm. Data are presented as mean ± SEM and are representative of two independent experiments. Symbols *, **, and * denote $p < 0.05$, $p < 0.01$, and $p < 0.001$, respectively.**

comparison to untreated cells up to 25 mg/mL. Altogether this suggests that pβCD NPs are not genotoxic.

We next investigated whether pβCD can induce inflammatory responses, using a highly sensitive dendritic cell maturation assay. Bone-marrow-derived dendritic cells (BMDC) were incubated for 24 h with different concentrations of pβCD, and the surface expression of CD40, CD80, and CD86, as well as of major histocompatibility complex (MHC)-class I or -II molecules, was studied by flow cytometry to assess the phenotypic maturation of BMDC. In contrast to the positive control, *Mycobacterium bovis* (Bacillus Calmette-Guerin, BCG) at a multiplicity of infection (MOI) of 1, which induced substantial up-regulation of these surface maturation markers (Figure 3C, right), pβCD did not modify the expression profile of these markers (Figure 3C, left). We also quantified the secretion of targeted cytokines by BMDM that had been incubated with different concentrations of pβCD. We observed that pβCD did not induce secretion of the inflammatory

DOI: 10.1021/acsnano.8b07902
ACS Nano 2019, 13, 3992−4007

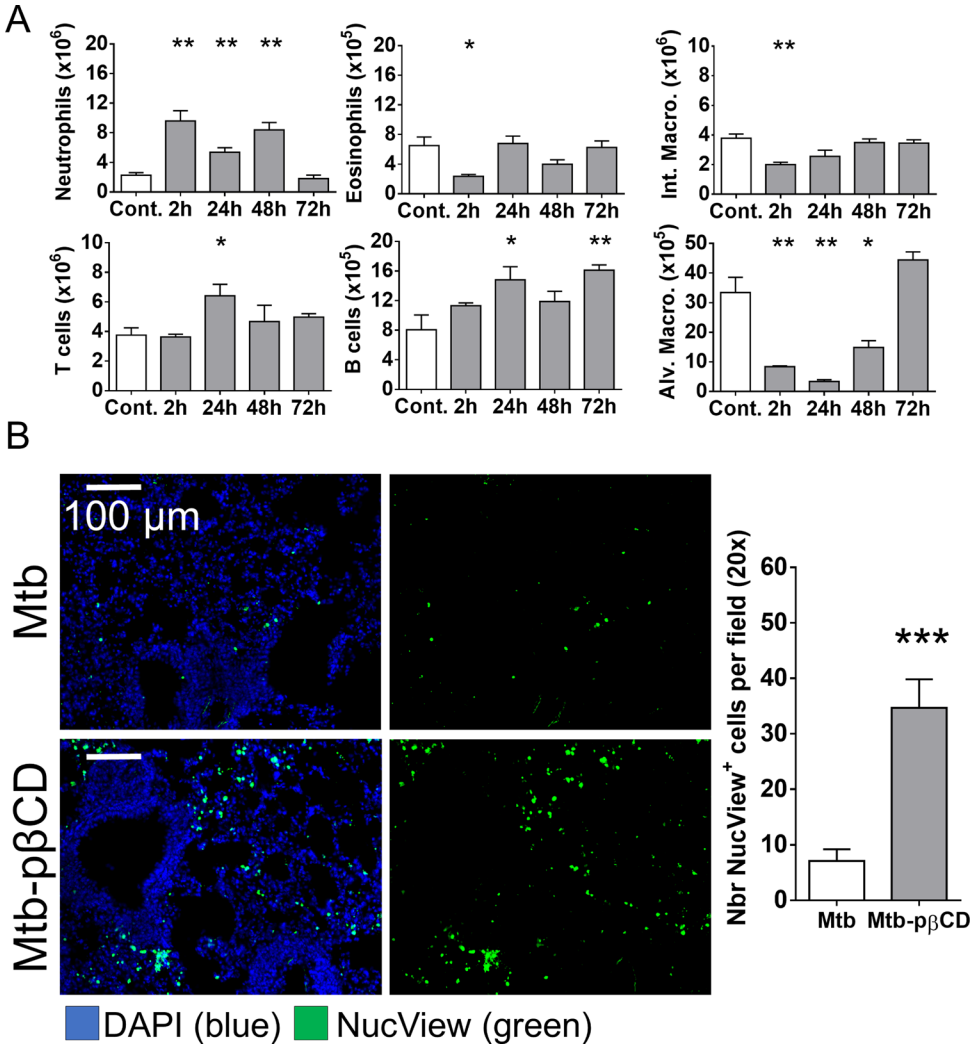

Figure 6. pβCD induce alveolar macrophage depletion and pulmonary apoptosis. (A) BALB/c mice received one i.n. administration of pβCD (150 mg/mL, 50 µL) and were euthanized at indicated time points postadministration to evaluate the number of different cell populations in lungs by flow cytometry. The following cell types were analyzed: alveolar macrophages ($CD11c^+$ $F4/80^+$ $SiglecF^+$), interstitial macrophages ($F4/80^+$ $CD11c^{int}$ $SiglecF^-$), neutrophils ($CD11b^+$ $LY6G^+$), eosinophils ($SiglecF^+$ $CD11c^-$), T cells ($CD3^+$), and B cells ($B220^+$ $MHCII^+$). (B) BALB/c mice were inoculated *via* the i.n. route with Mtb H37Rv (10^5 CFU). At days 7, 9, 11, 14, 16, and 18 postchallenge, mice received administrations of 50 µL of pβCD (150 mg/mL) *via* the e.t. route. At day 21 postchallenge, 50 µL of NucView 488 caspase-3 substrate (diluted in PBS) was administered i.n. to each mouse for 1 h before lung harvesting and subsequent fluorescence histology analysis. Data are presented as mean ± SEM and are representative of two independent experiments. Symbols *, **, and * denote $p < 0.05$, $p < 0.01$, and $p < 0.001$, respectively.**

cytokines TNF-α and IL-1β up to the concentration of 5 mg/mL. At 25 mg/mL, the production of IL-1β and TNF-α by BMDMs increased to 400 and 200 pg/mL, respectively, upon an overnight incubation with pβCD at 25 mg/mL, although their levels remained much lower than the positive control used here (BCG vaccine) with 1100 and 700 pg/mL, respectively. Altogether these results showed that pβCD had only very low pro-inflammatory effect at high concentration and no potential for inflammasome activation (Figure 3D).

pβCD Prevent Mtb Uptake by Macrophages *via* Cholesterol Depletion. It is well recognized that monomeric βCD affect the cholesterol content of plasma membranes and disturb lipid raft distribution.[32−35] We therefore examined the effect of pβCD on the BMDM plasma membrane using a green-fluorescent Cholera toxin B subunit (CTB-FITC) as a marker that binds to cholesterol and lipid rafts. BMDM were first incubated with various concentrations of pβCD and then labeled with CTB-FITC. In control macrophages, cholesterol was detected exclusively on the plasma membrane, whereas in pβCD-treated cells, cholesterol was depleted from the plasma membrane and distributed in a diffuse manner throughout the cytosol (Figure 4A), which indicates a translocation of plasma membrane cholesterol subsequent to pβCD treatment.

As cholesterol plays an essential role in the entry of mycobacteria into macrophages,[36,37] we wondered whether pβCD could affect the uptake of Mtb in cells. BMDM were first incubated with pβCD at various concentrations for either 2 or 16 h. After washing, red-fluorescent Mtb (H37Rv-pMRF1) was added at an MOI of 2. Two hours later, the cells were fixed and stained with DAPI (DNA marker), and the percentage of cells containing mycobacteria was determined by automated confocal microscopy and image analysis. Around 40% of BMDM harbored Mtb in control cells (Cont.), whereas less than 25% of pβCD-treated BMDM showed intracellular Mtb independent

DOI: 10.1021/acsnano.8b07902
ACS Nano 2019, 13, 3992−4007

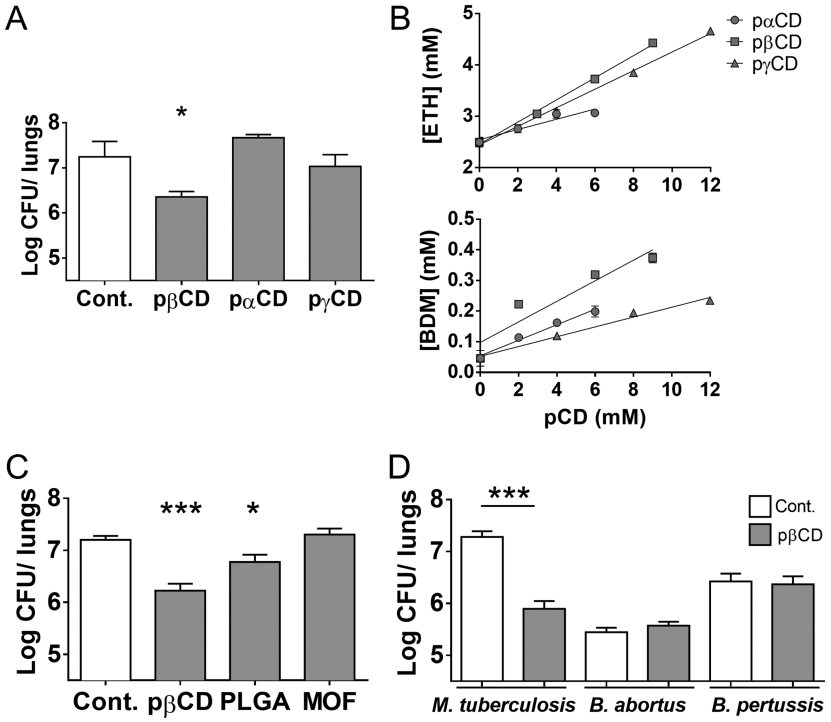

Figure 7. Effect of other types of nanoparticles on Mtb infection and effect of pβCD on other bacterial pulmonary diseases in mice. (A, C) BALB/c mice were infected *via* the i.n. route with 10^5 Mtb H37Rv (20 μL of PBS). At days 7, 9, 11, 14, 16, and 18 mice received pulmonary administration of nanoparticles in a volume of 50 μL (pαCD, pβCD, or pγCD 150 mg/mL, PLGA 15 mg/mL, MOF 5 mg/mL) 21 days postinfection. Lungs were harvested for bacterial burden evaluation by CFU counting. (B) Solubility properties of ETH and BDM43266 using pαCD, pβCD, and pγCD. (D) Mice were i.n. infected with the indicated bacteria. At defined days postinfection, mice received i.n. administration of pβCD (150 mg/mL, 50 μL) before CFU counting. Data are presented as mean ± SEM and are representative of two independent experiments. Symbols * and * denote $p < 0.05$ and $p < 0.001$, respectively.**

of the concentrations tested (Figure 4B,C). The effect was even more striking when BMDM had been preincubated with pβCD for 16 h (Figure 4D). Only 11% of BMDM were found infected in the presence of 2 mg/mL of pβCD. A maximal reduction of 7% was found at a pβCD concentration of 25 mg/mL. Thus, these data demonstrate that pβCD inhibit macrophage colonization *in vitro* by inducing the depletion of cholesterol at the plasma membrane. Our data suggest a direct correlation between the inhibition of the bacterial uptake *in vitro* and the reduced Mtb infection *in vivo*. This may be explained by the fact that the bacterium does not reach its intracellular niche, where replication occurs. It was also reported that lipid rafts are needed for translocation of innate immune receptors such as TLR2 during Mtb infection,[38] raising the hypothesis that cholesterol depletion by pβCD could impair innate immune responses against bacteria. These hypotheses deserve further investigation.

pβCD Impair *in Vitro* Mtb Replication and Induce Host Cell Apoptosis. We next investigated the abilities of pβCD to modulate the replication of Mtb inside macrophages. BMDM were infected with red-fluorescent Mtb (H37Rv-pMRF1) at an MOI of 2 for 4 h before extensive washing to remove extracellular bacteria. Twenty-four hours postinfection, cells were incubated with pβCD at concentrations ranging from 1 to 25 mg/mL during 5 days before being fixed, and the cell nuclei were labeled with DAPI. After image acquisition, a dedicated image analysis enabled the quantification of the bacterial area per infected cell, which is a biological correlate of infection corresponding to the bacterial load per cell (Figure 5A). In nontreated macrophages (Cont.), the bacterial area reached around 400 pixels^2 5 days postinfection. Interestingly, infected cells that were incubated with pβCD resulted in a bacterial area lower than 300 pixels^2, demonstrating that pβCD reduce Mtb replication.

Taking into account this observation, the cytosolic translocation of cholesterol (Figure 4A) and the fact that targeting cholesterol by βCD renders cells more sensitive to apoptosis,[32,33,39] we investigated whether treatment with pβCD is proapoptotic for macrophages. BMDM were incubated with various concentrations of pβCD for 24 h, prior to fixation and labeling with annexin V and a DNA intercalating dye. In this assay, necrotic cells are single positive for the DNA intercalating dye, while cells in early apoptosis are single positive for annexin V, and late apoptotic cells are double positive. While untreated BMDM were double negative in this assay, cells incubated with pβCD were single positive for annexin V, in contrast to the BMDM treated with staurosporine, which typically leads to late apoptotic, double-positive cells (Figure 5B,C). This effect is important to counteract the blockade of host cell apoptosis, previously reported for Mtb.[40] Moreover, Mtb eludes immunity and disseminates in a necrosis-dependent manner. Therefore, reprogramming the host cell death toward apoptosis can be detrimental to mycobacterial growth.[41] In addition, the host is able to kill bacteria through efferocytosis, by which Mtb-infected macrophages in apoptosis are rapidly phagocytized by uninfected bystander macrophages.[42]

pβCD Induce *in Vivo* Apoptosis in Lungs, Impairing Reservoirs for Mtb. We next studied the cell composition of lung immune cells after e.t. administration of pβCD. BALB/c mice ($n = 4$ per group) received *via* e.t. route 50 μL of pβCD at 150 mg/mL. At various time points postadministration, the cell

DOI: 10.1021/acsnano.8b07902
ACS Nano 2019, 13, 3992−4007

populations were studied by flow cytometry. As expected, an increase in the absolute number of neutrophils was observed early at 2 h postinoculation (Figure 6A). Slight decreases were observed in the absolute numbers of interstitial macrophages and eosinophils at 2 h, while an increase was detected in the absolute number of T and B lymphocytes, which were increased at 24 h postinoculation. Only the increase in B lymphocytes persisted until 72 h postinoculation. In contrast, inoculation of pβCD caused a 10-fold decrease in the number of alveolar macrophages as soon as 24 h postinoculation. This last observation, together with the previous results, suggested that pβCD were mainly ingested by alveolar macrophages, leading to their apoptotic death. To prove our hypothesis, the quantification of apoptotic cells in lungs of infected mice that had been previously treated with pβCD was performed. BALB/c mice were infected *via* i.n. route with Mtb and treated with pβCD (50 μL at 150 mg/mL) at days 7, 9, 11, 14, 16, and 18. At 21 days postinfection, mice were anesthetized and received *via* i.n. route the NucView 488 caspase-3 substrate that labels apoptotic cells. After 1 h, mice were euthanized, and their lungs were then fixed and prepared for histology. Samples were sliced into 10 μm sections and stained with DAPI for fluorescence microscopy analysis (Figure 6B). Results showed that pβCD administration increased 4 times the number of apoptotic cells in lungs of infected mice in comparison to nontreated, infected mice. Thus, our results suggest that pulmonary administration of pβCD may result in a transient but drastic depletion of alveolar macrophages by inducing apoptotic cell death.

Of note, the *in vivo* depletion of alveolar macrophages by pβCD treatment is rapid and transient, suggesting it has little impact on lung homeostasis. In support of our findings, a recent study showed that specific depletion of alveolar macrophages by pulmonary administration of liposomal formulations leads to a decrease of lung Mtb burden with similar efficacy to that for the pβCD treatment performed in the present study.[43]

pβCD Antibacterial Activity Is Specific for Mtb *in Vivo*. To establish whether such intrinsic inhibitory effect was specific to pβCD or shared by other nanocarriers, we expanded the study to other unloaded nanoparticles. First, we investigated the effect against an Mtb challenge of nanoparticles of poly-α-CD (pαCD) and poly-γ-CD (pγCD), for which no genotoxicity was observed (Supp. Figure 1). Interestingly, we observed that pβCD had an antibacterial activity but not pαCD or pγCD (Figure 7A).

Of note, the pαCD and pγCD NPs were less prone to solubilize both drugs (ETH and BDM43266) than pβCD (Figure 7B). As shown in Figure 7B, the apparent solubility of both ETH and Booster increased linearly by increasing pCD concentrations, which was also the case with native CDs (Supp. Figure 2). The phase solubility diagram was a typical AL-type, indicating the formation of soluble ETH/CD and Booster/CD complexes.[44] The obtained binding constants $K_{1:1}$ (M-1) of these complexes are shown in Supp. Table 1. All the CDs or pCDs were able to increase the apparent solubility of both drugs. Interestingly, it appears that both ETH and Booster are better accommodated in the cavity of βCD as compared to the other types of CDs, as shown by the obtained $K_{1:1}$ of 24, 100, and 47 for αCD, βCD, and γCD, respectively, in the case of ETH and 100, 514, and 256 in the case of Booster (Supp. Table 1). Compared to these native CD monomers, pCDs were more efficient in enhancing the apparent solubilities, especially for the Booster. For example, the $K_{1:1}$ of Booster was 100 for αCD and 503 for pαCD, which is possibly due to the contributions of hydrophobic microdomains formed in the cross-linked pβCD. In a nutshell, pβCD was the best among all tested CD-based materials to increase the apparent solubility of both drugs, achieving a $K_{1:1}$ of 110 and 1037 for ETH and Booster, respectively. Moreover, this polymer is highly water-soluble, allowing a dramatic increase of the apparent solubility of both ETH and Booster and avoiding crystallization issues.[18] Together, these results show that pβCD is a good candidate to study its intrinsic antibacterial activity.

We further investigated the intrinsic antimycobacterial properties of nanoparticles made of poly(lactic-*co*-glycolic acid) (PLGA), one of the most widely employed biomaterials for drug loading,[45,46] and the more recently developed highly porous hybrid nanoparticles made of metal−organic frameworks (nanoMOF).[47] PLGA nanoparticles and nanoMOFs were administered i.n. at the highest doses for which there was no aggregation. Subsequent to 6 i.n. administrations of NPs, we detected no effect on mycobacterial loads in nanoMOF-treated mice, but a slight decrease of 0.5-log in the bacterial loads in PLGA-treated mice, which however did not reach the observed rate in pβCD-treated mice (Figure 7C).

Finally, we sought to determine whether the antibacterial effect of pβCD was specific to tuberculosis bacilli. We thus evaluated the effect of pβCD on bacterial loads in mouse models of infection with (i) *Brucella abortus*, the causative agent of brucellosis, and (ii) *Bordetella pertussis*, the causative agent of whooping cough. *B. abortus* is a facultative intracellular Gram-negative coccobacillus that infects mammals and may cause fetus abortion. Human brucellosis is a zoonotic infection transmitted mainly through ingestion and inhalation.[48] *B. pertussis* is an extracellular bacterium causing whooping cough or pertussis, a severe respiratory disease that can be life-threatening in young infants. Both bacterial pathogens colonize the respiratory tract and persist several days in lungs after challenge. Administration of pβCD in the lung of mice infected with either *B. abortus* or *B. pertussis* had no impact on the bacterial load, as determined at day 14 and day 21 postchallenge, respectively, in contrast to the effects observed in the Mtb mouse model (Figure 7D). This suggests that pβCD act in a specific manner by interfering with macrophage colonization by Mtb. The absence of pβCD effect on *B. pertussis* may result from the fact that this pathogen, in contrast to Mtb, is an extracellular bacterium, and thus its *in vivo* replication is not directly dependent on macrophages impacted by the pβCD treatment. The fact that pβCD have no effect on the intracellular pathogen *B. abortus* underscores a cellular mechanism that is not common to other intracellular bacteria, which deserves more investigation. Thus, the antibacterial effect of pβCD in the lung is specific and helps host cells to control Mtb infection.

CONCLUSIONS

Current TB therapy is characterized by a complex drug regimen that needs to be taken for 6 months, causing problems of toxicity and compliance. Therefore, treating TB remains a challenge given the complexity and the lack of understanding of many aspects of the basic biology underlying this disease. The limitations of conventional therapies and the increasing incidence of MDR- and XDR-TB underpin the need for innovative therapeutic approaches. One of them consists of using nanotechnologies to combat microbial resistance.[21]

Taken together, we showed that e.t. administration of pβCD to Mtb-exposed mice leads to a decrease of Mtb burden, which is concomitant with reprogramming the properties of alveolar macrophages (Figure 8). Pulmonary administration of pβCD

DOI: 10.1021/acsnano.8b07902
ACS Nano 2019, 13, 3992−4007

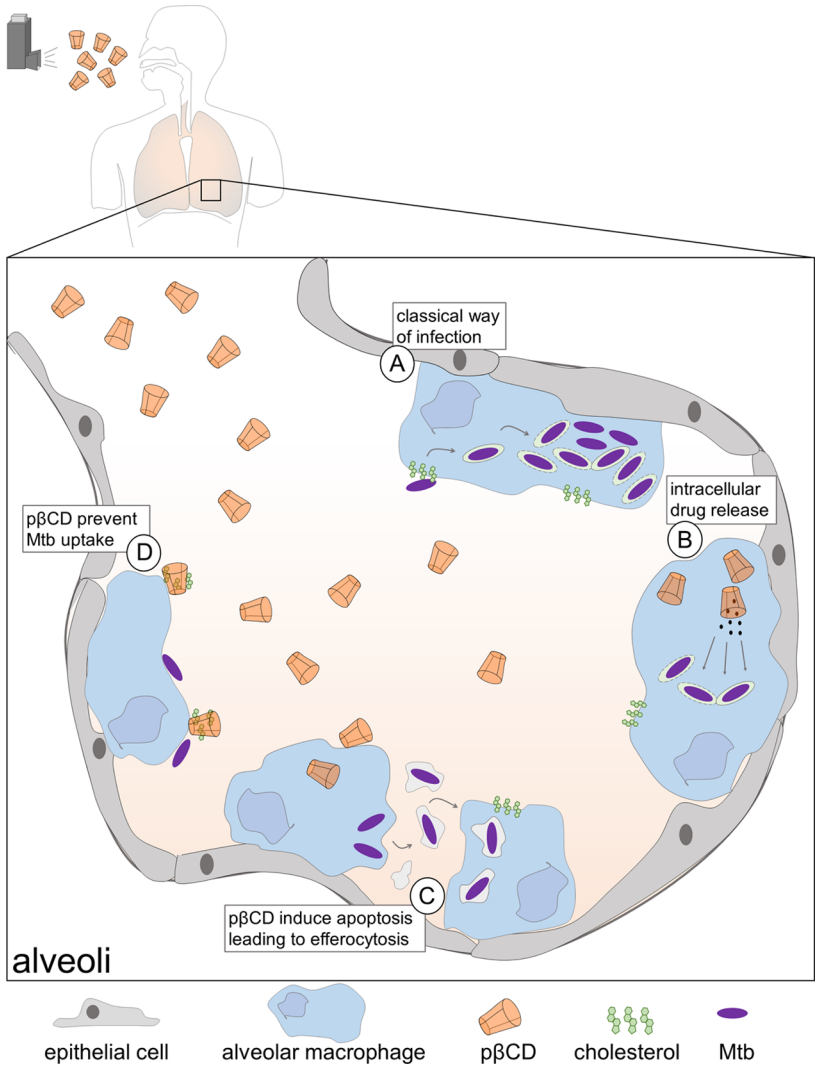

Figure 8. Model of antimycobacterial activities of pβCD within alveoli of infected lungs. (A) In the absence of treatment, Mtb uses cholesterol-rich lipid raft structures to invade alveolar macrophages. Then, Mtb interferes with the endocytic pathway to inhibit vacuolar acidification and to induce phagosomal rupture, enabling its replication. The decrease of the lung bacterial burden upon pβCD aerosolization is caused by three independent properties of the nanoparticle: (B) pβCD allows drug encapsulation for administration of nonsoluble molecules directly into the lung, the main site of Mtb infection. (C) pβCD induces host cell apoptosis, leading to efferocytosis, which is detrimental for Mtb establishment. (D) pβCD induces cholesterol depletion, impairing bacterial uptake.

induces transitory depletions of one of the main Mtb reservoir cells, which could contribute to the decrease of Mtb burden *via* efferocytosis of apoptotic alveolar macrophages containing surviving bacteria. Moreover, with the specific depletion of membrane cholesterol in alveolar macrophages, extracellular bacteria will be less likely to invade their neighboring cells. In summary, we identified a promising tool that not only improves drug bioavailability at the site of infection but also makes macrophages less permissive to Mtb replication. The search for new molecules able to boost host capacities for Mtb killing is considered as a promising strategy to counteract the limitation of current TB treatment and the appearance of MDR mycobacteria.[49] βCD-based NPs represent a potent drug carrier that could contribute to move this concept forward. This activity could fit into the emerging and promising concept of anti-TB approaches by host-directed therapy, which aims to empower host immune properties for the elimination of mycobacteria and/or for the reduction of tissue damage induced by the infection.[50]

METHODS

Nanoparticle Preparation. β-Cyclodextrin was kindly supplied by Roquette, Lestrem, France. pβCD nanoparticles of around 10 nm were produced as previously described[51,52] by cross-linking βCD under strongly alkaline conditions with epichlorohydrin (EP). Briefly, 100 g of anhydrous βCD was solubilized overnight in 160 mL of NaOH 33% w/w solution. After adding 81.52 g of EP, the reaction was stopped in the vicinity of the gelation point. The pβCD, recovered by ultrafiltration followed by freeze-drying, contained 70% w/w βCD, as determined by ^{1}H NMR spectroscopy. Using the same cross-linking method, αCD and γCD (Sigma-Aldrich, Saint Quentin Fallavier, France) were cross-linked, leading to the formation of pαCD and pγCD, respectively. These materials had similar properties except their CD content, which was 61% w/w and 82% w/w for pαCD and pγCD, respectively.

Nanoparticle preparations were purified using high-capacity endotoxin-free columns (ThermoFisher). For both cellular and *in vivo* experiments, pβCD were dispersed in water. For the various cellular assays, nanoparticles were harvested in microplates, and manual dilutions of the mother solution in a final volume of 100 μL were performed in sterile Milli-Q water in a 384 deep well "diamond plate" (Axygen) in order to obtain a dose−response curve. Previously, 5 μL of

DOI: 10.1021/acsnano.8b07902
ACS Nano 2019, 13, 3992−4007

each concentration of the pβCD were dispensed in 384-well clear-bottom polystyrene assay plates (Greiner Bio-One). Water was used as negative control (Cont). Rhod-pβCD were synthesized according to a previously reported method.[53]

Nanoparticles of porous nanoMOF MIL-100(Fe) (MIL stands for Material of Institut Lavoisier) were synthesized by microwave-assisted hydrothermal reaction as previously described.[54] A mixture containing the iron source (iron(III) chloride hexahydrate) (6.0 mmol) and the organic bridging ligand (1,3,5-benzenetricarboxylic acid) (4.02 mmol) was heated in 20 mL of deionized water, 6 min at 130 °C under stirring. The reaction was carried out in a Pyrex reactor at a power of 800 W (Mars-5, CEM, US). The crystalline iron-trimesate nanoMOFs were recovered by centrifugation (15 min, 10000*g*) and purified by washing six times with absolute ethanol. The nanoparticles had a mean diameter of 225 nm and a specific BET surface of 1650 m^2/g, in agreement with previously reported data.[47] For *in vivo* administration, nanoMOF were administrated dispersed in water at a concentration of 5 mg/mL.

Poly(D,L-lactide-*co*-glycolide) (50:50 acid terminated, MW: 5−20 kDa, 10P019) was kindly provided by PCAS (Expansorb, Aramon, France). Nanoparticles were produced by an emulsification method as described in our previous study.[13] Their mean diameter was 180 nm. For *in vivo* experiments, PLGA were administrated at a concentration of 15 mg/mL.

Ethionamide and Booster Co-incorporation and Phase Solubility Studies. A series of CD aqueous solutions (0, 3, 6, and 9 mM for αCD, βCD, pβCD, and γCD; 0, 2, 5, and 7 mM for pαCD and 0, 4, 8, and 12 mM for pγCD) were introduced in vials containing excess amounts of ETH and Booster, respectively. The dispersions, accurately protected from light, were kept under shaking for 3 days for drug:CD complexation to reach equilibrium. Then, the excess (not dissolved) drugs were removed by centrifugation to obtain saturated ETH- or Booster-loaded systems. Drugs in the supernatants were extracted by adding equal volumes of a DMSO/acetonitrile (1:10 v/v) mixture, followed by centrifugation at 17000*g* for 20 min to remove the precipitated CDs or NPs. Drug concentration in the clear supernatants was assessed by RP-HPLC as previously described.[18] An Agilent HPLC system (Agilent 1100 Series) equipped with a C_{18} column (Kinetex 5 μm, 100A, Phenomenex) and a UV detector at 280 nm was used. The eluants were as follows: solvent A 0.1% trifluoroacetic acid (TFA) in Milli-Q water and solvent B 0.1% TFA in acetonitrile; 0−2 min: 0−20% B, 2−6 min: 20−45% B, 6−10 min: 45−75% B, 10−15 min: 75−0%. The flow rate was 1.0 mL/min at room temperature.

Phase solubility diagrams were obtained by plotting the apparent solubility of ETH or Booster against the equivalent molar CDs' concentrations. For pCDs, the concentrations were calculated taking into account their CD content determined by NMR. Assuming a 1:1 stoichiometry of the binding interactions, the binding constants ($K_{1:1}$) were calculated from the linear regression curve of solubility diagrams, according to the following equation:[44]

$$K_{1:1} = \frac{\text{slope}}{S_0(1 - \text{slope})}$$

S_0 determines drug solubility in water.

For *in vitro* and *in vivo* studies, ETH and Boosters (BDM43266 and BDM 41906) were encapsulated in pCDs without using any organic solvent, by mixing overnight 150 mg of pCD suspensions with the drug powders, 3 mg of ETH, and 3 mg of Booster per mL of water as previously described.[18]

Mice. Six-week-old Balb/c female mice and C57BL/6 female mice were purchased from Janvier (Le Genest-Saint-Isle, France) and were maintained in the animal facility of the Pasteur Institute of Lille, France (Agreement B59-350009). The project received ethical approval by the French Committee on Animal Experimentation and the Ministry of Education and Research (00579.01 approved on December 2, 2015, and APAFIS#10232-2017061411305485 v6 approved in September 2018). All experiments were performed in accordance with relevant guidelines and regulations.

Murine Bone-Marrow Macrophages and Dendritic Cells. Murine bone-marrow progenitors were obtained by sampling tibias and femur bones from 7- to 11-week-old C57BL/6 mice. BMDM and BMDC were obtained by seeding 10^7 bone marrow cells in 75 cm^2 flasks in RPMI 1640 Glutamax medium (Gibco) supplemented with 10% heat-inactivated fetal bovine serum (FBS) (Gibco) and 10% L929-conditioned medium containing macrophage colony-stimulating factor (M-CSF) or granulocyte-macrophage colony-stimulating factor (GM-CSF). After 7 days' incubation at 37 °C and 5% CO_2, BMDM were rinsed with Dulbecco's phosphate-buffered saline (D-PBS) and harvested with Versene (Gibco) to be used for the following assays.

CTB-FITC Staining and Apoptosis Assay. A total of 10^4 BMDM were seeded in 384-well plates in the presence of various concentrations of pβCD diluted in 50 μL of RPMI containing 10% FBS and M-CSF. After an overnight incubation with pβCD, BMDM were fixed with 10% neutral buffered formalin solution (HT5014) containing 4% paraformaldehyde for 30 min and then labeled with CTB-FITC (C1655) and DAPI at 10 μg/mL in D-PBS for 10 min at room temperature (RT). The GFP-certified apoptosis/necrosis detection kit (Enzo, ENZ-51002) was used to monitor cell death. Confocal images were acquired using an Opera automated confocal microscope (PerkinElmer), and image quantification was performed using Columbus software.

Mtb Entry or Replication Assay. Recombinant Mtb H37Rv expressing the red fluorescent protein DsRed (H37Rv-pMRF1)[55] was cultured at 37 °C for 2 weeks in Middlebrook 7H9 medium (Difco) supplemented with 10% Middlebrook oleic acid-albumin-dextrose-catalase (OADC, Difco), 0.5% glycerol (Sigma-Aldrich), 0.05% Tween 80 (Sigma-Aldrich), and 20 μg/mL kanamycin (Invitrogen). Mycobacteria were washed three times with D-PBS (free of $MgCl_2$ and $CaCl_2$, Gibco) and resuspended in RPMI-1640 Glutamax medium containing 10% heat-inactivated FBS (Life Technologies). Clumped mycobacteria were removed by centrifugation at 700 rpm for 2 min, and homogeneous supernatants were used for infection. Bacterial titer was determined by measuring the red fluorescence on a Victor multilabel counter (PerkinElmer) and a standard titration curve. The bacterial suspension was diluted at 2×10^6 CFU per mL in RPMI 1640 supplemented with 10% FBS (RPMI-FBS) before being added to BMDM for infection.

For the Mtb entry assay, bacteria were added to BMDM that had been incubated for 2 or 16 h with various dilutions of pβCD. At 2 h postinfection, cells were fixed with 10% neutral buffered formalin solution (Sigma-Aldrich) for 30 min and then labeled with DAPI at 10 μg/mL in D-PBS for 10 min at RT for image-based analysis.

For the Mtb replication assay, BMDM were infected during 24 h (MOI 2) before being incubated with various concentrations of pβCD until day 5 postinfection. Then, cells were fixed with 10% neutral buffered formalin solution (Sigma-Aldrich) for 30 min and then labeled with DAPI at 10 μg/mL in D-PBS for 10 min at RT for image-based analysis.

Image Acquisition and Image-Based Analysis. For intracellular assays, image acquisition of 384-well plates was performed on an automated fluorescent confocal microscope (InCell6000, GE Healthcare), using a 20× objective. The confocal microscope was equipped with 405, 488, 561, and 640 nm excitation lasers. A series of six fields was taken per well, and each one was analyzed using the image-analysis software Columbus (version 2.5.1, PerkinElmer). Cells (nuclei and cytoplasm) were detected by an intensity detection algorithm applied on the DAPI channel. A spot detection algorithm based on the RFP channel was applied for the detection of Mtb-pMRF1 in cells, and the bacterial intensity and area in pixels were measured. Images were analyzed to determine the percentage of infected cells.

Genotoxicity Assay. THP1 (ATCC TIB-202) cells were incubated for 4 h in complete medium with different concentrations of pCD suspensions in sterile water or positive controls as described.[56] For the *in vitro* micronucleus assay, cells were washed and reincubated for a 1.5−2 cell cycle recovery period. At the end of this recovery period, cells were washed and trypsinized. After centrifugation at 1000 rpm (95*g*) for 6 min, supernatant was discarded and cells were treated with a hypotonic solution (culture medium diluted 1:1 in distilled water). After the hypotonic shock, a prefixation step was performed by adding cold Carnoy's fixative (methanol/glacial acetic acid, 3:1 v/v). Cells

DOI: 10.1021/acsnano.8b07902
ACS Nano 2019, 13, 3992−4007

were then centrifuged and suspended in Carnoy's fixative for 10 min. After another centrifugation, cells were resuspended and spread on duplicate glass slides. Slides were air-dried overnight and stained for 10 min with 4% v/v Giemsa in water. Micronuclei, identified according to recommended criteria, were scored at 500× magnification in 1000 intact mononucleated cells per slide. The comet assay was performed under alkaline conditions (pH > 13). At the end of the 4 h treatment, THP1 cells were washed and trypsinized. Trypsin was inactivated by adding complete medium. Viable cells were counted using Trypan blue exclusion, and 8×10^4 viable cells were mixed with 0.5% w/v low melting point agarose (LMPA) kept at 37 °C. Cells embedded in LMPA were spread on regular precoated microscopy slides (1.5% and 0.8% w/v normal melting point agarose). All the following steps were sheltered from daylight to prevent the occurrence of additional DNA damage. Slides were immersed for at least 1 h at 4 °C in a cold lysing solution (2.5 M NaCl, 100 mM EDTA, 10 mM Trizma base, pH 10, supplemented with 1% v/v Triton X-100 and 10% v/v dimethyl sulfoxide). All slides were then placed in a horizontal tank filled with fresh electrophoresis solution (1 mM EDTA and 300 mM NaOH, pH > 13) for 20 min to allow DNA unwinding and expression of strand breaks and alkali-labile sites. Next, electrophoresis was performed for 20 min using an electric current of 0.7 V cm^{-1}. Slides were then placed for 10 min in a neutralization solution (0.4 M Trizma base, pH 7.5), and gels were dehydrated by immersion in absolute ethanol for 5 min. Finally, slides were air-dried and stored at room temperature. Slides were independently coded and analyzed after addition of propidium iodide (20 μg/mL) and a coverslip on each slide. Slides were then examined at 250× magnification using a fluorescence microscope (Leica Microscopy and Scientific Instruments Group, Heerbrugg, Switzerland) equipped with an excitation filter of 515−560 nm and a 590 nm barrier filter, connected through a gated CCD camera to Comet Image Analysis System software, version 4.0 (Perceptive Instruments Ltd., Haverhill, UK). One hundred randomly selected cells were scored on each slide, corresponding to 200 cells.

Dendritic Cell Maturation Assay. BMDC were incubated with 1 or 2 mg/mL of pβCD overnight. *M. bovis* BCG1173P2, a strong inducer of DC maturation, was used as positive control. Cells were washed and incubated with anti-CD16/CD32 (2.4G2 mAb, BD Pharmingen) during 20 min followed by surface staining during a 20 min incubation with appropriate dilutions of PE-Cy7-anti-CD11c in combination with FITC-conjugated anti-CD40 (HM40-3, SONY), anti-CD80 (B7-1) (16-10A1 Biolegend), anti-CD86 (B7-2) (PO3, SONY), anti-MHCII (I-A/I-E) (MS/114.15.2, eBioscience), anti-MHC-I ($H\text{-}2k^b$) (AF6-88-5-5-3, eBioscience), or the control Ig isotype antibodies. The stained cells were washed twice in PBS containing 3% FBS and 0.1% NaN_3 and then fixed with 4% paraformaldehyde during 18 h at 4 °C prior to sample acquisition by a CytoFlex cytometer system (Beckman Coulter). As a functional DC maturation assay, TNF-α and IL-1β were quantified by ELISA in the culture supernatants of the same cultures, as described.[57]

Effect of pβCD on Mtb-Infected Mice. Eight-week-old BALB/c mice (4 mice per group) were inoculated with Mtb H37Rv *via* the i.n. route (10^5 CFU/20 μL) as described.[13] Briefly, 50 μL of water containing pβCD (or PBS alone as control) was administered to mice *via* the e.t. route using a microsprayer (MicroSprayer Aerosolizer model IA-1C-M and FMJ-250 high-pressure syringe, Penn Century Inc., Wyndmoor, PA, USA) or *via* the i.n. route. Administrations were performed on day 7, 9, 11, 14, 16, and 18. At day 21, mice were euthanized and lungs were homogenized using the MM300 bead beater (Retsch), and 10-fold serial dilutions were plated onto 7H11 agar plates supplemented with 10% OADC. CFUs were determined after a three-week growth period at 37 °C.

Effect of pβCD on *B. abortus*-Infected Mice. As described,[58] 8-week-old BALB/c mice were i.n. infected by *B. abortus* 2308 (10^5 CFU in 30 μL). Cultures were grown overnight with shaking at 37 °C in 2YT medium (Luria−Bertani broth with double quantity of yeast extract) and were washed twice in RPMI 1640 (Gibco Laboratories) (3500*g*, 10 min) before inoculation of the mice. The mice were anesthetized with a cocktail of xylazine (9 mg/kg) and ketamine (36 mg/kg) in PBS before being inoculated. The infectious doses were validated by plating serial dilutions of the inoculum; i.n. administrations of pβCD were performed on day 7, 9, 11, 14, 16, and 18. The mice were sacrificed 21 days after infection by cervical dislocation. Immediately after sacrifice, lungs were collected for bacterial counts. Organs were crushed and transferred to PBS/0.1% X-100 Triton (Sigma-Aldrich). We performed successive serial dilutions in RPMI and plated them onto 2YT medium. The CFUs were determined after 5 days of culture at 37 °C.

pβCD Effect on *B. pertussis*-Infected Mice. Groups of 4 or 5 BALB/c mice (8-weeks-old) were sedated with pentobarbital (CEVA Santé Animale, La Ballastière, France) and i.n. infected with 20 μL of PBS containing 10^6 CFU of *B. pertussis*. The *B. pertussis* strain used was streptomycin-resistant BPSM and was grown on Bordet-Gengou agar (Difco Laboratories) supplemented with 1% glycerol, 20% defibrinated sheep blood, and 100 μg/mL streptomycin at 37 °C as described.[59] After growth, the bacteria were collected and resuspended in PBS at the desired density; i.n. administrations of pβCD was performed on day 1, 3, and 6. Seven days postinfection, lungs were harvested, homogenized in PBS, and plated in serial dilutions onto BG-blood agar for CFU quantification after 5 days of incubation at 37 °C.

Flow Cytometry Analysis of Lungs. Harvested organs were cut into small pieces and incubated for 1 h at 37 °C with a mix of DNase I (100 μg/mL, Sigma-Aldrich) and collagenase D (400 U/mL, Roche). Lung cells were washed and filtered before being incubated with saturating doses of purified 2.4G2 (anti-mouse Fc receptor, ATCC) in 200 μL of PBS, 0.2% BSA, and 0.02% NaN_3 (FACS buffer) for 20 min at 4 °C to prevent antibody binding to Fc receptors. Various fluorescent monoclonal antibody (mAb) combinations in FACS buffer were used to stain (3−5) × 10^6 cells. Acquisitions were done on a FACScanto II cytofluorometer (Becton Dickinson) with the following mAbs: fluorescein (FITC)-coupled anti-CD3 (145-2C11, BD Biosciences), FITC-coupled anti-CD11c (HL3, ThermoFisher), FITC-coupled anti LY6G (1A8, BD Biosciences), phycoerythrine (PE)-coupled anti-SiglecF (E50-2440, BD Biosciences), PE-coupled anti-MHCII (M5, BD Biosciences), PE-coupled anti CD11b (M1/70, BD Biosciences), allophycocyanin (APC)-coupled anti-F4/80 (BM8, BD Biosciences), APC-coupled anti-B220 (RA3-6B2, BD Biosciences), APC-coupled anti-CD11c (HL3, BD Biosciences), Brillant violet 421 (BV421)-coupled anti SiglecF (E50-2440, BD Biosciences), BV421-coupled anti-MHCII (M5, BD Biosciences). Fixable viability dye aqua (ThermoFisher) was used to gate viable cells.

Fluorescent Histology on Infected Lung and Apoptosis Staining. Mice were anesthetized and *via* i.n. administrated with 50 μL of NucView 488 caspase-3 substrate (Ozyme) diluted in PBS (250×). One hour after injection, mice were euthanized to harvest lungs for histological analysis. In detail, lungs were fixed overnight at 4 °C with 10% neutral buffered formalin solution (Sigma-Aldrich), washed in PBS, and incubated overnight at RT in a 20% PBS/sucrose solution under vacuum. Tissues were then embedded in the Tissue-Tek OCT compound (Sakura) and frozen in liquid nitrogen, and cryostat sections (10 μm) were prepared. For staining, tissue sections were rehydrated in PBS and incubated in a PBS solution containing 1% blocking reagent (Boeringer) (PBS-BR 1%) and DAPI nucleic acid stain for 20 min. Slides were mounted in Fluoro-Gel medium (Electron Microscopy Sciences, Hatfield, PA, USA). Labeled tissue sections were visualized with an Axiovert M200 inverted microscope (Zeiss, Iena, Germany) equipped with a high-resolution monochrome camera (AxioCam HR, Zeiss). At least three slides were analyzed per organ from three different animals, and the results are representative of two independent experiments.

Statistical Analysis. A Mann−Whitney test was applied using GraphPad Prism software. Each group of mice was compared to the control group. Comparison of groups two-by-two was performed, and the results are displayed when required. Values of $p < 0.05$ were considered significant. Indicated symbols of *, **, and *** denote $p < 0.05$, $p < 0.01$, and $p < 0.001$, respectively.

DOI: 10.1021/acsnano.8b07902
ACS Nano 2019, 13, 3992−4007

ASSOCIATED CONTENT

Supporting Information

The Supporting Information is available free of charge on the ACS Publications website at DOI: 10.1021/acsnano.8b07902.

Additional information (PDF)

AUTHOR INFORMATION

Corresponding Authors

*E-mail: ruxandra.gref@u-psud.fr.

*E-mail: priscille.brodin@inserm.fr.

ORCID

Ruxandra Gref: 0000-0002-7869-0908

Priscille Brodin: 0000-0003-0991-7344

Present Address

□Present address: Institut Pasteur, Theravectys Joint Lab, 28 Rue du Dr. Roux, F-75015 Paris, France.

Author Contributions

The author(s) have made the following declarations about their contributions: Conceived and designed the experiments: A.M., G.S., L.M., R.G., P.B. Performed the experiments: A.M., G.S., X.L., A.D., A.S.D., M.M.M., E.P., S.J., E.H., N.D., I.B., C.R., S.S., S.T., V.G., F.N., L.M., R.G., P.B. Contributed reagents/materials/analysis tools: A.M., G.S., X.L., M.M.M., E.H., N.D., B.V., M.F., R.B., F.N., B.D., E.M., C.L., A.R.B., N.W., R.G., P.B. Performed data analysis: A.M., L.M., F.N., R.G., P.B. Wrote the paper: A.M., E.H., L.M., R.G., P.B.

Notes

The authors declare no competing financial interest.

ACKNOWLEDGMENTS

We gratefully acknowledge F. Leroux, H. Bauderlique, O. R. Song, I. Ricard, and A. Vandeputte for technical assistance and helpful discussions. We also acknowledge R. Prath, N. Vandenabeele, and D. Legrand for technical assistance in BSL3 and animal facilities. We are grateful to Roquette for kindly providing us with a sample of β-cyclodextrin. We acknowledge the PICT-IBiSA and F. Lafont from BiCEL for providing access to microscopy equipment. Financial support for this work was provided by the European Community (CycloNHit no. 608407, ERC-STG INTRACELLTB no. 260901, MM4TB no. 260872), the Agence Nationale de la Recherche (ANR-10-EQPX-04-01, ANR-14-CE08-0017, ANR-16-CE35-0009), the Projet Transversal de l'Institut Pasteur (PTR441, PTR22-16), the EMBO Young Investigator Program, the Feder (12001407 (D-AL) Equipex Imaginex BioMed), the Région Hauts-de-France (convention no. 12000080), and the Fondation pour la Recherche Medicale (SPF20170938709). This work was supported by a public grant overseen by the French National Research Agency (ANR) as part of the "Investissements d'Avenir" program (Labex NanoSaclay, ANR-10-LABX-0035).

REFERENCES

(1) WHO. *Global Tuberculosis Report 2018*. 2018.

(2) Gandhi, N. R.; Nunn, P.; Dheda, K.; Schaaf, H. S.; Zignol, M.; van Soolingen, D.; Jensen, P.; Bayona, J. Multidrug-Resistant and Extensively Drug-Resistant Tuberculosis: a Threat to Global Control of Tuberculosis. *Lancet* **2010**, *375*, 1830−1843.

(3) Queval, C. J.; Brosch, R.; Simeone, R. The Macrophage: A Disputed Fortress in the Battle Against *Mycobacterium tuberculosis*. *Front. Microbiol.* **2017**, *8*, 2284−2295.

(4) Prideaux, B.; Via, L. E.; Zimmerman, M. D.; Eum, S.; Sarathy, J.; O'Brien, P.; Chen, C.; Kaya, F.; Weiner, D. M.; Chen, P. Y.; Song, T.; Lee, M.; Shim, T. S.; Cho, J. S.; Kim, W.; Cho, S. N.; Olivier, K. N.; Barry, C. E., 3rd; Dartois, V. The Association Between Sterilizing Activity and Drug Distribution Into Tuberculosis Lesions. *Nat. Med.* **2015**, *21*, 1223−1227.

(5) Hickey, A. J.; Durham, P. G.; Dharmadhikari, A.; Nardell, E. A. Inhaled Drug Treatment for Tuberculosis: Past Progress and Future Prospects. *J. Controlled Release* **2016**, *240*, 127−134.

(6) Dakal, T. C.; Kumar, A.; Majumdar, R. S.; Yadav, V. Mechanistic Basis of Antimicrobial Actions of Silver Nanoparticles. *Front. Microbiol.* **2016**, *7*, 1831−1848.

(7) Chen, W.; Cheng, C. A.; Lee, B. Y.; Clemens, D. L.; Huang, W. Y.; Horwitz, M. A.; Zink, J. I. A Facile Strategy Enabling Both High Loading and High Release Amounts of the Water-insoluble Drug Clofazimine Using Mesoporous Silica Nanoparticles. *ACS Appl. Mater. Interfaces* **2018**, *10*, 31870−31881.

(8) Huo, S.; Jiang, Y.; Gupta, A.; Jiang, Z.; Landis, R. F.; Hou, S.; Liang, X. J.; Rotello, V. M. Fully Zwitterionic Nanoparticle Antimicrobial Agents through Tuning of Core Size and Ligand Structure. *ACS Nano* **2016**, *10*, 8732−8737.

(9) Fenaroli, F.; Repnik, U.; Xu, Y.; Johann, K.; Van Herck, S.; Dey, P.; Skjeldal, F. M.; Frei, D. M.; Bagherifam, S.; Kocere, A.; Haag, R.; De Geest, B. G.; Barz, M.; Russell, D. G.; Griffiths, G. Enhanced Permeability and Retention-like Extravasation of Nanoparticles From the Vasculature Into Tuberculosis Granulomas in Zebrafish and Mouse Models. *ACS Nano* **2018**, *12*, 8646−8661.

(10) Fenaroli, F.; Westmoreland, D.; Benjaminsen, J.; Kolstad, T.; Skjeldal, F. M.; Meijer, A. H.; van der Vaart, M.; Ulanova, L.; Roos, N.; Nystrom, B.; Hildahl, J.; Griffiths, G. Nanoparticles as Drug Delivery System Against Tuberculosis in Zebrafish Embryos: Direct Visualization and Treatment. *ACS Nano* **2014**, *8*, 7014−7026.

(11) Pelgrift, R. Y.; Friedman, A. J. Nanotechnology as a Therapeutic Tool to Combat Microbial Resistance. *Adv. Drug Delivery Rev.* **2013**, *65*, 1803−1815.

(12) Pancani, E.; Menendez-Miranda, M.; Pastor, A.; Brisset, F.; Bernet-Camard, M. F.; Desmaele, D.; Gref, R. Nanoparticles With High Payloads of Pipemidic Acid, a Poorly Soluble Crystalline Drug: Drug-Initiated Polymerization and Self-Assembly Approach. *Acta Pharm. Sin. B* **2018**, *8*, 420−431.

(13) Costa-Gouveia, J.; Pancani, E.; Jouny, S.; Machelart, A.; Delorme, V.; Salzano, G.; Iantomasi, R.; Piveteau, C.; Queval, C. J.; Song, O. R.; Flipo, M.; Deprez, B.; Saint-Andre, J. P.; Hureaux, J.; Majlessi, L.; Willand, N.; Baulard, A.; Brodin, P.; Gref, R. Combination Therapy for Tuberculosis Treatment: Pulmonary Administration of Ethionamide and Booster Co-Loaded Nanoparticles. *Sci. Rep.* **2017**, *7*, 5390−5404.

(14) Willand, N.; Dirié, B.; Carette, X.; Bifani, P.; Singhal, A.; Desroses, M.; Leroux, F.; Willery, E.; Mathys, V.; Déprez-Poulain, R. Synthetic EthR Inhibitors Boost Antituberculous Activity of Ethionamide. *Nat. Med.* **2009**, *15*, 537−544.

(15) Russell, D. G.; Huang, L.; VanderVen, B. C. Immunometabolism at the Interface Between Macrophages and Pathogens. *Nat. Rev. Immunol.* **2019**, s41577−019−0124.

(16) Baulard, A. R.; Betts, J. C.; Engohang-Ndong, J.; Quan, S.; McAdam, R. A.; Brennan, P. J.; Locht, C.; Besra, G. S. Activation of the Pro-Drug Ethionamide is Regulated in Mycobacteria. *J. Biol. Chem.* **2000**, *275*, 28326−28331.

(17) Villemagne, B.; Flipo, M.; Blondiaux, N.; Crauste, C.; Malaquin, S.; Leroux, F.; Piveteau, C.; Villeret, V.; Brodin, P.; Villoutreix, B. O.; Sperandio, O.; Soror, S. H.; Wohlkonig, A.; Wintjens, R.; Deprez, B.; Baulard, A. R.; Willand, N. Ligand Efficiency Driven Design of New Inhibitors of *Mycobacterium tuberculosis* Transcriptional Repressor EthR Using Fragment Growing, Merging, and Linking Approaches. *J. Med. Chem.* **2014**, *57*, 4876−4888.

(18) Salzano, G.; Wankar, J.; Ottani, S.; Villemagne, B.; Baulard, A. R.; Willand, N.; Brodin, P.; Manet, I.; Gref, R. Cyclodextrin-Based Nanocarriers Containing a Synergic Drug Combination: A Potential Formulation for Pulmonary Administration of Antitubercular Drugs. *Int. J. Pharm.* **2017**, *531*, 577−587.

(19) Daoud-Mahammed, S.; Couvreur, P.; Bouchemal, K.; Cheron, M.; Lebas, G.; Amiel, C.; Gref, R. Cyclodextrin and Polysaccharide-

DOI: 10.1021/acsnano.8b07902
ACS Nano 2019, 13, 3992−4007

Based Nanogels: Entrapment of Two Hydrophobic Molecules, Benzophenone and Tamoxifen. *Biomacromolecules* **2009**, *10*, 547−554.
(20) Andrade, F.; Rafael, D.; Videira, M.; Ferreira, D.; Sosnik, A.; Sarmento, B. Nanotechnology and Pulmonary Delivery to Overcome Resistance in Infectious Diseases. *Adv. Drug Delivery Rev.* **2013**, *65*, 1816−1827.
(21) Costa-Gouveia, J.; Ainsa, J. A.; Brodin, P.; Lucia, A. How Can Nanoparticles Contribute to Antituberculosis Therapy? *Drug Discovery Today* **2017**, *22*, 600−607.
(22) Gnanadhas, D. P.; Ben Thomas, M.; Thomas, R.; Raichur, A. M.; Chakravortty, D. Interaction of Silver Nanoparticles With Serum Proteins Affects Their Antimicrobial Activity *In Vivo*. *Antimicrob. Agents Chemother.* **2013**, *57*, 4945−4955.
(23) Maronpot, R. R.; Hobbs, C. A.; Davis, J.; Swartz, C.; Boyle, M.; Koyanagi, M.; Hayashi, S. M. Genetic and Rat Toxicity Studies of Cyclodextrin Glucanotransferase. *Toxicol. Rep.* **2016**, *3*, 381−392.
(24) Kurkov, S. V.; Loftsson, T. Cyclodextrins. *Int. J. Pharm.* **2013**, *453*, 167−180.
(25) Shelat, R.; Chandra, S.; Khanna, A. Detailed Toxicity Evaluation of Beta-Cyclodextrin Coated Iron Oxide Nanoparticles for Biomedical Applications. *Int. J. Biol. Macromol.* **2018**, *110*, 357−365.
(26) Bivas-Benita, M.; Ottenhoff, T. H.; Junginger, H. E.; Borchard, G. Pulmonary DNA Vaccination: Concepts, Possibilities and Perspectives. *J. Controlled Release* **2005**, *107*, 1−29.
(27) Misra, A.; Hickey, A. J.; Rossi, C.; Borchard, G.; Terada, H.; Makino, K.; Fourie, P. B.; Colombo, P. Inhaled Drug Therapy for Treatment of Tuberculosis. *Tuberculosis* **2011**, *91*, 71−81.
(28) Sharma, A.; Sharma, S.; Khuller, G. K. Lectin-Functionalized Poly (Lactide-Co-Glycolide) Nanoparticles as Oral/Aerosolized Antitubercular Drug Carriers for Treatment of Tuberculosis. *J. Antimicrob. Chemother.* **2004**, *54*, 761−766.
(29) Stella, V. J.; He, Q. Cyclodextrins. *Toxicol. Pathol.* **2008**, *36*, 30−42.
(30) Elespuru, R.; Pfuhler, S.; Aardema, M. J.; Chen, T.; Doak, S. H.; Doherty, A.; Farabaugh, C. S.; Kenny, J.; Manjanatha, M.; Mahadevan, B.; Moore, M. M.; Ouedraogo, G.; Stankowski, L. F., Jr.; Tanir, J. Y. Genotoxicity Assessment of Nanomaterials: Recommendations on Best Practices, Assays, and Methods. *Toxicol. Sci.* **2018**, *164*, 391−416.
(31) Udroiu, I.; Sgura, A. Cytogenetic Tests for Animal Production: State of the Art and Perspectives. *Anim. Genet.* **2017**, *48*, 505−515.
(32) Yamaguchi, R.; Perkins, G.; Hirota, K. Targeting Cholesterol With Beta-Cyclodextrin Sensitizes Cancer Cells for Apoptosis. *FEBS Lett.* **2015**, *589*, 4097−4105.
(33) Badana, A. K.; Chintala, M.; Gavara, M. M.; Naik, S.; Kumari, S.; Kappala, V. R.; Iska, B. R.; Malla, R. R. Lipid Rafts Disruption Induces Apoptosis by Attenuating Expression of LRP6 and Survivin in Triple Negative Breast Cancer. *Biomed. Pharmacother.* **2018**, *97*, 359−368.
(34) Zidovetzki, R.; Levitan, I. Use of Cyclodextrins to Manipulate Plasma Membrane Cholesterol Content: Evidence, Misconceptions and Control Strategies. *Biochim. Biophys. Acta, Biomembr.* **2007**, *1768*, 1311−1324.
(35) Hinzey, A. H.; Kline, M. A.; Kotha, S. R.; Sliman, S. M.; Butler, E. S.; Shelton, A. B.; Gurney, T. R.; Parinandi, N. L. Choice of Cyclodextrin for Cellular Cholesterol Depletion for Vascular Endothelial Cell Lipid Raft Studies: Cell Membrane Alterations, Cytoskeletal Reorganization and Cytotoxicity. *Indian J. Biochem. Biophys.* **2012**, *49*, 329−341.
(36) Gatfield, J.; Pieters, J. Essential Role for Cholesterol in Entry of Mycobacteria Into Macrophages. *Science* **2000**, *288*, 1647−1650.
(37) Munoz, S.; Rivas-Santiago, B.; Enciso, J. A. *Mycobacterium tuberculosis* Entry Into Mast Cells Through Cholesterol-Rich Membrane Microdomains. *Scand. J. Immunol.* **2009**, *70*, 256−263.
(38) Shin, D. M.; Yang, C. S.; Lee, J. Y.; Lee, S. J.; Choi, H. H.; Lee, H. M.; Yuk, J. M.; Harding, C. V.; Jo, E. K. *Mycobacterium tuberculosis* Lipoprotein-Induced Association of TLR2 With Protein Kinase C Zeta in Lipid Rafts Contributes to Reactive Oxygen Species-Dependent Inflammatory Signalling in Macrophages. *Cell. Microbiol.* **2008**, *10*, 1893−1905.
(39) Chen, Y. C.; Gowda, R.; Newswanger, R. K.; Leibich, P.; Fell, B.; Rosenberg, G.; Robertson, G. P. Targeting Cholesterol Transport in Circulating Melanoma Cells to Inhibit Metastasis. *Pigm. Cell Melanoma Res.* **2017**, *30*, 541−552.
(40) Schaaf, K.; Smith, S. R.; Duverger, A.; Wagner, F.; Wolschendorf, F.; Westfall, A. O.; Kutsch, O.; Sun, J. *Mycobacterium tuberculosis* Exploits the PPM1A Signaling Pathway to Block Host Macrophage Apoptosis. *Sci. Rep.* **2017**, *7*, 42101−42117.
(41) Lam, A.; Prabhu, R.; Gross, C. M.; Riesenberg, L. A.; Singh, V.; Aggarwal, S. Role of Apoptosis and Autophagy in Tuberculosis. *Am. J. Physiol.* **2017**, *313*, 218−229.
(42) Martin, C. J.; Booty, M. G.; Rosebrock, T. R.; Nunes-Alves, C.; Desjardins, D. M.; Keren, I.; Fortune, S. M.; Remold, H. G.; Behar, S. M. Efferocytosis is an Innate Antibacterial Mechanism. *Cell Host Microbe* **2012**, *12*, 289−300.
(43) Huang, L.; Nazarova, E. V.; Tan, S.; Liu, Y.; Russell, D. G. Growth of *Mycobacterium tuberculosis In Vivo* Segregates With Host Macrophage Metabolism and Ontogeny. *J. Exp. Med.* **2018**, *215*, 1135−1152.
(44) Saokham, P.; Muankaew, C.; Jansook, P.; Loftsson, T. Solubility of Cyclodextrins and Drug/Cyclodextrin Complexes. *Molecules* **2018**, *23*, 1161−1176.
(45) Petros, R. A.; DeSimone, J. M. Strategies in the Design of Nanoparticles for Therapeutic Applications. *Nat. Rev. Drug Discovery* **2010**, *9*, 615−627.
(46) Shive, M. S.; Anderson, J. M. Biodegradation and Biocompatibility of PLA and PLGA Microspheres. *Adv. Drug Delivery Rev.* **1997**, *28*, 5−24.
(47) Horcajada, P.; Chalati, T.; Serre, C.; Gillet, B.; Sebrie, C.; Baati, T.; Eubank, J. F.; Heurtaux, D.; Clayette, P.; Kreuz, C.; Chang, J. S.; Hwang, Y. K.; Marsaud, V.; Bories, P. N.; Cynober, L.; Gil, S.; Ferey, G.; Couvreur, P.; Gref, R. Porous Metal-Organic-Framework Nanoscale Carriers as a Potential Platform for Drug Delivery and Imaging. *Nat. Mater.* **2010**, *9*, 172−178.
(48) Godfroid, J.; Cloeckaert, A.; Liautard, J. P.; Kohler, S.; Fretin, D.; Walravens, K.; Garin-Bastuji, B.; Letesson, J. J. From the Discovery of the Malta Fever's Agent to the Discovery of a Marine Mammal Reservoir, Brucellosis Has Continuously Been a Re-Emerging Zoonosis. *Vet. Res.* **2005**, *36*, 313−326.
(49) Machelart, A.; Song, O. R.; Hoffmann, E.; Brodin, P. Host-Directed Therapies Offer Novel Opportunities for the Fight Against Tuberculosis. *Drug Discovery Today* **2017**, *22*, 1250−1257.
(50) Kaufmann, S. H. E.; Dorhoi, A.; Hotchkiss, R. S.; Bartenschlager, R. Host-Directed Therapies for Bacterial and Viral Infections. *Nat. Rev. Drug Discovery* **2017**, *17*, 35−56.
(51) Gref, R.; Amiel, C.; Molinard, K.; Daoud-Mahammed, S.; Sebille, B.; Gillet, B.; Beloeil, J. C.; Ringard, C.; Rosilio, V.; Poupaert, J.; Couvreur, P. New Self-Assembled Nanogels Based on Host-Guest Interactions: Characterization and Drug Loading. *J. Controlled Release* **2006**, *111*, 316−324.
(52) Othman, M.; Bouchemal, K.; Couvreur, P.; Desmaele, D.; Morvan, E.; Pouget, T.; Gref, R. A Comprehensive Study of the Spontaneous Formation of Nanoassemblies in Water by a "Lock-and-Key" Interaction Between Two Associative Polymers. *J. Colloid Interface Sci.* **2011**, *354*, 517−527.
(53) Aykac, A.; Noiray, M.; Malanga, M.; Agostoni, V.; Casas-Solvas, J. M.; Fenyvesi, E.; Gref, R.; Vargas-Berenguel, A. A Non-Covalent "Click Chemistry" Strategy to Efficiently Coat Highly Porous MOF Nanoparticles With a Stable Polymeric Shell. *Biochim. Biophys. Acta, Gen. Subj.* **2017**, *1861*, 1606−1616.
(54) Rodriguez-Ruiz, V.; Maksimenko, A.; Anand, R.; Monti, S.; Agostoni, V.; Couvreur, P.; Lampropoulou, M.; Yannakopoulou, K.; Gref, R. Efficient "Green" Encapsulation of a Highly Hydrophilic Anticancer Drug in Metal-Organic Framework Nanoparticles. *J. Drug Targeting* **2015**, *23*, 759−767.
(55) Deboosere, N.; Iantomasi, R.; Queval, C. J.; Song, O. R.; Deloison, G.; Jouny, S.; Debrie, A. S.; Chamaillard, M.; Nigou, J.; Cohen-Gonsaud, M.; Locht, C.; Brodin, P.; Veyron-Churlet, R. LppM

DOI: 10.1021/acsnano.8b07902
ACS Nano 2019, 13, 3992−4007

Impact on the Colonization of Macrophages by *Mycobacterium tuberculosis*. *Cell. Microbiol.* **2017**, *19*, No. e12619.
(56) Moche, H.; Chevalier, D.; Vezin, H.; Claude, N.; Lorge, E.; Nesslany, F. Genotoxicity of Tungsten Carbide-Cobalt (WC-Co) Nanoparticles *In Vitro*Mechanisms-of-Action Studies. *Mutat. Res., Genet. Toxicol. Environ. Mutagen.* **2015**, *779*, 15−22.
(57) Sayes, F.; Sun, L.; Di Luca, M.; Simeone, R.; Degaiffier, N.; Fiette, L.; Esin, S.; Brosch, R.; Bottai, D.; Leclerc, C.; Majlessi, L. Strong Immunogenicity and Cross-Reactivity of *Mycobacterium tuberculosis* ESX-5 Type VII Secretion: Encoded PE-PPE Proteins Predicts Vaccine Potential. *Cell Host Microbe* **2012**, *11*, 352−363.
(58) Machelart, A.; Khadrawi, A.; Demars, A.; Willemart, K.; De Trez, C.; Letesson, J. J.; Muraille, E. Chronic *Brucella* Infection Induces Selective and Persistent Interferon Gamma-Dependent Alterations of Marginal Zone Macrophages in the Spleen. *Infect. Immun.* **2017**, *85*, 115−117.
(59) Feunou, P. F.; Kammoun, H.; Debrie, A. S.; Locht, C. Heterologous Prime-Boost Immunization With Live Attenuated *B. pertussis* BPZE1 Followed by Acellular Pertussis Vaccine in Mice. *Vaccine* **2014**, *32*, 4281−4288.

DOI: 10.1021/acsnano.8b07902
ACS Nano 2019, 13, 3992−4007